Silicate cloud formation in the atmospheres of close-in super-Earths and gas giants

by

Gourav Mahapatra
Student number: 4413385

in partial fulfillment of the requirements for the degree of

Master of Science
in Aerospace Engineering

at the Delft University of Technology.

September 5, 2016

Project Supervisor:	Dr. Ch. Helling,	University of St. Andrews
TU Delft Supervisor:	Dr. D. M. Stam,	TU Delft
Thesis committee:	Dr. L. L. A. Vermeersen,	TU Delft
	Dr. A. Menicucci,	TU Delft



Contents

1 Introduction **7**

2 Deriving the starting composition of planetary atmospheres **10**
2.1 Conversion of weight(%) of oxides to element abundances in H scale. 11

3 Equilibrium chemistry **15**
3.1 Equilibrium chemistry model 15
3.2 Inputs 17

4 Atmospheric composition of close-in Super Earths and giant gas planets **18**
4.1 Giant gas planet atmosphere 18
4.2 Atmospheres of Hot Super-Earths (CoRoT-7b) 20
4.3 Possible atmosphere on 55 Cnc e 23
4.4 The atmosphere on HD149026b 23
4.5 Summary: Atmosphere composition 30

5 Cloud formation on highly irradiated planets of non-solar composition **31**
5.1 Cloud formation process 31
5.2 Cloud model and Input Quantities 33
5.3 Atmospheric mixing 33

6 Cloud formation results **35**

7 Discussions and Summary **37**

List of Figures

1 Abundance of various elements... 13
2 Temperature Vs. Pressure profiles of different objects considered for this study... . . 16
3 Thoretical T_{eq} vs. log P_{eq} for five types of HRSE models with increasing T_{eq}. 21
4 Gas-phase compositions in relative abundance with respect to Hyodrogen 22
5 as-phase compositions of some dominant species such as Ti, Si, Mg, Fe, Al resulting from a Solar and a BSE compositions. 24
6 Concentration vs. Pressure plot for 'Si' Silicate species resulting from equilibrium chemistry for four types of elements abundances 25
7 Concentration vs. Pressure plot for "Ti" Silicate species resulting from equilibrium chemistry for four types of elements abundances 26
8 Concentration vs. Pressure plot for 'Fe' Silicate species resulting from equilibrium chemistry for four types of elements abundances 27
9 Concentration vs. Pressure plot for 'Mg' Silicate species resulting from equilibrium chemistry for four types of elements abundances. 28
10 Concentration vs. Pressure plot for 'Al' Silicate species resulting from equilibrium chemistry for four types of elements abundances 29
11 DRIFT cloud model results for Giant Planet 41
12 Dust grain properties resulting from cloud formations on a hot Giant Planet 42
13 DRIFT cloud model results for 55Cnc e 43
14 Dust grain properties resulting from cloud formations on a sample atmosphere for 55 Cnc e 44
15 DRIFT cloud model results for HD149026b 45
16 Dust grain properties resulting from cloud formations on a sample atmosphere for HD149026b 46
17 DRIFT cloud model results for CoRoT-7b 47

List of Tables

1 Weight (%) of oxides found in various types of Earth and magma rocks. 11
2 Showing element abundances for six types of magma compositions with Solar and meteorite abundances. 12
3 Characteristics of the modelled planets. (All values are approximations of recent findings.) 15
4 List of 20 most abundant species in gas-phase compostions resulting from atmospheric equilibrium chemistry of 1. Gas Giant (T_{eff}=2500 K), 2. 55 Cnc e(T_{eq}=2400 K), 3. HD149026b(T_{eq}=1757K) and 4. CoRoT-7b(T_{eq}=2300 K), arranged according to their decreasing concentration in the atmosphere for Solar and BSE types of element abundances as listed in Table 2. 20
5 Added surface reactions for the growth of dust particles. The solids resulting from these reactions are indicated with an [s] in the **rhs** of the reaction. 32
6 Dust volume fractions (V_s/V_{tot} [%]) in percentages for individual growth species, Maximum nucleation rates and particle sizes contributing to the dust formation in three types of compositions. We show the cloud properties in three different stages of its evolution i.e. at cloud Top (where TiO_2 nucleation begins), at the middle (approximate half-length of the cloud) and at the cloud Base (where the dust species evaporate). 38

List of Abbreviations

BSE	Bulk Silicate Earth
BC	Bulk Crust
UC	Upper Crust
MORB	Metal Oxide rich Basalt
HRSE	Hot Rocky Super Earth

Abstract

Context: Clouds form in the atmospheres of brown dwarfs and extrasolar planets. Recent observations of planets orbiting extremely close (<0.1 AU) to their stars indicate possible atmospheres with silicate compositions resulting due to vaporization of silicate magma from their surface. Such atmospheres are heavily dependent on compositions of the planetary crust which in turn might influence the kind of dust particles that form in such atmospheres.
Aims: We identify five types of silicate compositions commonly found on Earth and derive atmospheric chemistry with Earth silicates as starting compositions using an equilibrium chemistry atmospheric model. Following the mineral cloud modelling approach for hot atmospheres of brown dwarfs and giant gas planets, we model the dust cloud formations resulting due to varying Earth silicate compositions and apply that to investigate the possibility of clouds on sample atmospheres of a giant gas planet, 55 Cnc e, HD149 026b and CoRoT-7b.
Methods: Atmospheric compositions for the planets have been derived using a previously validated Equilibrium chemistry code. We derive our atmospheric chemistry using element abundances from previously studied Earth surface compositions which is provided as an input to the 1D kinetic cloud formation model, DRIFT. We perform cloud modelling on each of the atmospheres with varying silicate compositions and study the resulting cloud properties such as particle growth, particle sizes and their composition at various stages.
Results: We present the cloud structures resulting due to varying Earth silicate compositions on four different types of planets. The clouds show variations in the dust properties due to different starting compositions with differing average particle sizes but the formation conditions such as average particle size, cloud thickness and condensation altitude largely remain dependent on the local gas density and temperature. The cloud layers on 55 Cnc e, HD149 026b are found to be greatly varying in terms of their geometrical thickness, particle sizes and number densities and are primarily composed of silicates of elements such as Mg, Si, Fe and Al.

1 Introduction

With telescopes of high-sensitivity and sophistication in place, we have ventured into an era of observing and characterizing the atmospheres of exoplanets in greater detail. Characterizing the atmospheres of these observable exoplanets is the first step towards identifying habitable planets. While observational characterization relies on powerful telescopes and inference of the received spectra, the principles that govern the atmospheric chemistry and compositions follow the same principles of thermodynamics and chemistry as seen here on Earth. Theoretical modelling of such atmospheres gives us an idea of the type of chemistry that would be possible in such a planet which would in-turn help in fitting our observed spectra. The study of atmospheres involves taking into account the characteristics of host-star, composition of the planet in consideration and the local gas temperatures and pressures amongst many other variables. (Knutson et al., 2007) and Fortney et al. (2007), Valencia et al. (2007) are a few examples of developed theoretical models for exoplanetary atmospheres. Giant gas planets orbiting close to their stars are the easiest to detect using the radial velocity method which causes timely fluctuations in the parent stars received spectra because of its "wobble". They are also the ones that are warm enough to be directly imaged (for e.g. GJ 504 b, (Kuzuhara et al., 2013)). Some examples of well studied close-in giant gas planets are HD 189733 b, CoRoT-1b (Snellen et al., 2009) and HAT-P-1b (Bakos et al., 2007). Exoplanets such as CoRoT-7b (Léger et al., 2009), Kepler-10b (Batalha et al., 2011), Kepler-78b (Howard et al., 2013) with masses $\leq 10 M_{\oplus}$ are examples of super-Earths orbiting very close to their stars that have been able to retain atmospheres despite their close proximity to their stars. These kinds of planets with extremely high surface temperatures shall be referred to as Hot Rocky Super-Earths (HRSE, hereafter) (Ito et al., 2015).

The atmospheric composition of a planet strongly depends on the region of protoplanetary disk where it formed during the early stage of disk evolution. The likeliness of formation of giant gas planets is high near the snow-line of the system and beyond where, after the initial core accretion of solid mass of $\sim$10 $M_{\oplus}$, the planet accretes hydrogen and helium rich nebular gas to form gas giants (Madhusudhan et al., 2016). Some of these planets after solid mass accretion remain in the region within the snow-line and do not accrete enough volatiles but still retain volatiles enough to form an atmosphere and are commonly referred to as hot-Neptunes. Planets that remain close to their stars in early stages of planetary evolution would also have their atmospheres enriched by the vaporized surface materials (Schaefer and Fegley, 2009b). There is also a possibility of giant or semi giant gas planets migrating inwards due to various gravitational interactions after their initial formation beyond the snow line (Madhusudhan et al., 2014). The observation and characterization of atmospheres enriched possibly with surface silicates would provide us with an opportunity to study the internal composition of the planetary crusts and surface materials which would influence the observed spectra.

Schaefer and Fegley (2009b), developed a model for possible compositions of the "Silicate Atmosphere" that is in gas-melt equilibrium with the molten rocky surface with no highly volatile elements such as H, C, N, S and Cl. They considered temperatures, T, of 1500-3000 K and surface gravity of 36.2 ms^{-2} corresponding to the planetary properties for CoRoT-7b. They have assumed several compositions for the volatile-free magma for the formation of the atmospheres such as the Earth's continental and oceanic crusts, the Bulk Silicate Earth (BSE). Miguel et al. (2011b) explore

the composition of initial planetary atmospheres of HRSE's in the Kepler planet candidate sample, according to their semi-major axis. They used the MAGMA code developed by Schaefer and Fegley (2004) which calculates the equilibrium between the melt and the vapor in a magma exposed at temperatures higher than 1000 K, for Al, Ca, Fe, K, Mg, Na, O, Si, Ti and their compounds. Ito et al. (2015) conducted a similar survey with a few more types of Earth rocks. They went further and calculated the full radiative properties of one such atmosphere, which includes calculation of the absorption opacities from the absorption-line data for the major gas species. They consider line absorption by seven major species that include Na, K, Fe, O, O_2, Si and SiO.

Atmospheres hot enough (>1000 K) to have silicates of elements such as Si, Na, K, Fe, Al etc. in vapour state have the possibility of cloud formations from such gases when the gas-phase is sufficiently supersaturated. Brown Dwarfs are examples of intrinsically hot atmospheres where dust clouds form from the minerals present in gas state. Such clouds are responsible for altering the observed spectra by flattening the Ultra-violet(UV) and visible spectrum due to scattering from small sized particles, having a cooling effect on the atmosphere beneath the optically thick region by reflecting the received spectra and also by depleting the local gas-phase of minerals to condense and form dust particles (Woitke and Helling, 2003). Woitke and Helling (2003), Woitke and Helling (2004), Helling et al. (2008) are some examples of detailed theoretical modelling of mineral dust clouds on brown dwarf atmospheres and the resulting synthetic spectra. In a similar manner, hot Jupiters, hot Neptunes and HRSE atmospheres have the possibility of cloud formations provided suitable local gas temperature and pressures. For instance, the transit spectra of HD189733b from *Hubble* Space Telescope between 0.3 μm and 1.6 μm, is suggested by Des Etangs et al. (2008) to be consistent with a Rayleigh scattering from the atmosphere caused due to clouds/haze with cloud particles of $MgSiO_3$[s] and estimate a particle radii of $10^{-2}...10^{-1}$ μm at $\sim 10^{-6}...10^{-3}$ bar local pressure. Lee et al. (2015) use the kinetic cloud modelling approach of Helling et al. (2008) to derive 3D clouds model for the atmosphere of HD189733b. They find the dust clouds to be composed of stable condensates such as $MgSiO_3$[s], TiO_2[s], $CaTiO_3$[s], MgO[s], Fe[s] and also find the cloud particle sizes and compositions varying with different locations on the planet due to large temperature and pressure changes. Possibility of clouds have been proposed for super-Earth GJ436 b wherein the observed spectrum in 1.2 -1.6 μm is featureless indicating a possibility of "heavier than hydrogen" gas-phase molecular composition resulting in high opacity clouds that form at a pressure altitude of $\sim 10^{-3}$ bars (Knutson et al., 2014). Similarly Kreidberg et al. (2014) rule out the possibility of a cloud-free and volatile-rich atmosphere for GJ1214 b. Schaefer and Fegley (2009a) suggest clouds of Na and K gases in the upper parts of the atmosphere of CoRoT-7b which is a HRSE.

This study is inspired by the possibility of cloud formations in the various mentioned planetary atmospheres and investigates the possibility of mineral clouds on silicate-rich atmospheres. We analyze various Earth-like silicate rich atmospheric compositions and perform cloud modelling using the 1D kinetic cloud model, DRIFT. The resulting differences in the cloud properties due to changing element abundances have been analyzed. Section 2 describes the method adopted to derive Earth-like silicate compositions and the conversion method to obtain the element abundances. Section 3 describes the atmospheric chemistry and the code used to derive the gas-phase compositions of the various potential extrasolar planets based on their converged T,P profiles. Section 4 describes the derived gas-phase chemistry for the selected planetary T,P profiles, **Gas Giant** and three extra-solar planets, **CoRoT-7b**, **55 Cnc e** and **HD149026b**. Section 5 describes the cloud model used to perform the cloud modelling and the model parameters and inputs. It also describes the method of atmospheric mixing followed in this work to derive the clouds. Section 6 provides results obtained

for the modelling of clouds on four planetary scenarios and describes the cloud and dust properties obtained. Section 7 provides the discussions and summary for the obtained cloud formation results.

2 Deriving the starting composition of planetary atmospheres

We follow the procedure adopted by Schaefer and Fegley (2009a) in their work to derive the atmospheric composition of Super-Earths i.e. we assume that the atmosphere is enriched with elements from the vaporization of the planetary surface due to extremely high temperatures. Schaefer and Fegley (2009a); Miguel et al. (2011a); Ito et al. (2015) derive their planetary composition by taking into consideration, the composition of various magma and silicate rocks that are found on Earth. Miguel et al. (2011) have used two types of rock compositions, **Komatiite** and **bulk silicate earth** (BSE^b) for modelling their hot rocky super-earth's atmosphere. They have derived the compositions for Komatiite from Schaefer and Fegley (2004). The BSE compositions for their model is derived from the work by O'Neill & Palme (1998). Ito et al. (2015) have carried out a similar study where they have analysed four types of possible magma compositions (BSE^c, MORB, Bulk Crust, Upper Crust) for their radiative-transfer modelling of atmospheres of hot rocky super-earths. Rudnick & Gao (2003) provide a comprehensive estimate of the composition of earth's continental crust. The compositions for **Upper Crust** and **Lower Crusts** are derived from Taylor and McLennan (2009). The **mid-ocean rich basalt** (MORB) is found in active volcanic regions on Earth. The MORB composition is provided in McDonough and s. Sun (1995).

Earth's crust is mostly formed due to igneous processes and it's composition is distinct from the magma rocks because they are richer with incompatible elements. Incompatible element is an element that is unsuitable in size and/or charge to the cation sites of the minerals. Upper crust is the most accessible and consists of high percentages of incompatible elements. Bulk composition of the crust is an important geophysical parameter to study because it contains a sizeable fraction of the whole earth budget for many incompatible elements (Taylor and McLennan, 2009). The estimates can vary quite a lot depending upon the estimation method adopted. Although crustal composition is quite recent compared to the molten-lava rocks, we chose to carry out the atmospheric composition study for both cases. Table 1 lists the five types of rocks that have been chosen for this work which represent various possible compositions of Earth during its evolutionary period.

Table 1: Weight (%) of oxides found in various types of Earth and magma rocks.

Oxide (%)	Komatiite[a]	BSE[b]	BSE[c]	MORB[c]	Upper Crust[d]	Bulk Crust[d]
SiO_2	47.10	45.97	45.1	49.6	66.6	60.6
MgO	29.60	36.66	37.9	9.75	2.5	4.
FeO	-	8.24	8.06	8.06	5.04	6.71
Al_2O_3	4.04	4.77	4.46	16.8	15.4	15.9
CaO	5.44	3.78	3.55	12.5	3.59	6.40
Na_2O	0.46	0.35	0.36	2.18	3.27	3.07
Cr_2O_3	-	-	0.38	0.07	0.0003	0.0004
TiO_2	0.24	0.18	0.2	0.9	0.64	0.72
K_2O	0.09	0.04	0.03	0.07	2.8	1.81
P_2O_5	-	-	0.02	0.1	0.13	0.15
Fe_2O_3	12.8	-	-	-	-	-

[a] Schaefer and Fegley (2004), [b] O'Neill & Palme (1998), [c] McDonough and s. Sun (1995), [d] Taylor and McLennan (2009).

2.1 Conversion of weight(%) of oxides to element abundances in H scale.

It is a common convention found in geoscience literature to express the composition of a rock, in terms of weight of various compounds. This is expressed in weight percentage of a particular compound, for example the upper crust of the Earth is a mixture of 66.6 % SiO_2, 15.4 % Al_2O_3, 3.59 % CaO which are the major constituents among other compounds mentioned in Table 1. Such compositions are used to study and model the atmospheres of evaporating planets with surface temperatures above 1000 K. Table 1 lists the constituents that are commonly found in various types of Earth's crustal and magma rocks.

In astronomical literature, element abundances are not expressed as weight oxides(%) but rather in terms of, concentrations per 10^{12} H atoms. We calculate the abundance using the following equation,

$$\log(\epsilon_{\rm i}) = \log(\frac{\rm n_i}{\rm n_H}) + 12. \tag{1}$$

where $\epsilon_{\rm i}$ is the abundance of an element, i = Si, O, Mg..., n_i [cm^-3] = number density of the element i, $n_H = 10^{12}$. Therefore it is important to convert the abundances in weight oxides to elemental abundances expressed in the $\log(\epsilon_{\rm H}) = 12$ scale.

The weight oxide(%) of each compound(where compound is SiO_2, FeO,Al_2O_3 etc.) is used to calculate the number of moles of that compound in a particular rock type which can be calculated as,

$$\rm M(No.ofmoles) = \frac{m(\%ofCompound)}{n(MolarMass(g/mole))}. \tag{2}$$

The number of moles of a particular element, for eg. Oxygen(O) in SiO_2 is calculated using the following equation,

$$M_O = x_O.M \tag{3}$$

where "x" is the stoichiometric coefficient of the chosen element in the compound. We find the total number of atoms of a particular element by using the equation 4,

$$N_{tot,i} = (\sum x_a M_{i,a}) N_A. \tag{4}$$

$n_{tot,i}$ is the total number of moles of a particular element in the mixtures, a is the compound type (for eg., SiO_2, Al_2O_3, FeO, etc.) and N_A(atoms/mole) is the Avogadro's number.

The element abundances in the solar or cosmic scale are expressed relative to the number of H atoms. This is not possibe in case of a hot rocky planet's atmosphere because of the potential absence of H atoms. Thus, we follow the method generally used to calculate the element abundances in the case of meteorites. The abundance ratios are calculated with respect to the Si atoms in a scale of $\log_{10}$ Si = 6.

$$\log(\epsilon_{Si}) = \log(\frac{n_{tot,i}}{n_{Si}}) + 6. \tag{5}$$

Table 2: Showing element abundances for six types of magma compositions with Solar and meteorite abundances.

Element Abundance $\log(\epsilon_i/\epsilon_H)$	Komatiite[a]	BSE[b]	BSE[c]	MORB[c]	Upper Crust[d]	Bulk Crust[d]	Solar[e]	Meteorite[e]
Si	7.54	7.54	7.54	7.54	7.54	7.54	7.54	7.55
O	8.09	8.10	8.10	7.97	8.00	7.97	8.69	8.43
Mg	7.52	7.62	7.64	7.01	6.61	6.29	7.54	7.56
Fe	6.86	6.72	6.72	6.68	6.51	6.34	7.45	7.49
Ca	6.63	6.48	6.46	6.42	6.59	6.30	6.36	6.33
Al	6.54	6.62	6.61	6.57	7.03	6.97	6.47	6.46
Na	5.82	5.71	5.73	5.69	6.53	6.52	6.33	6.30
Ti	5.12	5.01	5.06	5.66	5.49	5.39	5.02	4.95
K	4.93	4.56	4.47	4.79	6.12	6.27	5.08	5.11
Cr	-	-	5.36	4.62	-	-	5.64	5.67
P	-	-	4.12	4.77	4.79	4.82	5.36	5.44

[a] Schaefer and Fegley (2004), [b] O'Neill & Palme (1998), [c] McDonough and s. Sun (1995), [d] Taylor and McLennan (2009). [e] Grevesse et al. (2007).

To be able to convert the Si-normalized abundances to a H-normalized abundances scale, we follow the method outlined by Palme et al. (2013). The conversion factor between the two scales was calculated by dividing the H-normalized solar abundances by the Si-normalized meteorite abundances. The comparison was made for all elements with an error of the corresponding photospheric abundance of less than 0.1 dex, i.e., less than ,25%. The log of the average ratio of solar abundance per 10^{12} H atoms/meteorite abundance per 10^6 silicon atoms is 1.546 ± 0.045(Palme et al., 2013). Here, we make an assumption that the meteorite compositions would be similar to the composition of a planet without any volatiles. Thus,

$$\log(\epsilon_H) = \log(\epsilon_{Si}) + 1.546 \tag{6}$$

Equation 6 provides us with the element abundances in the $\log(\epsilon_H) = 12$ scale which are listed in the table 2.

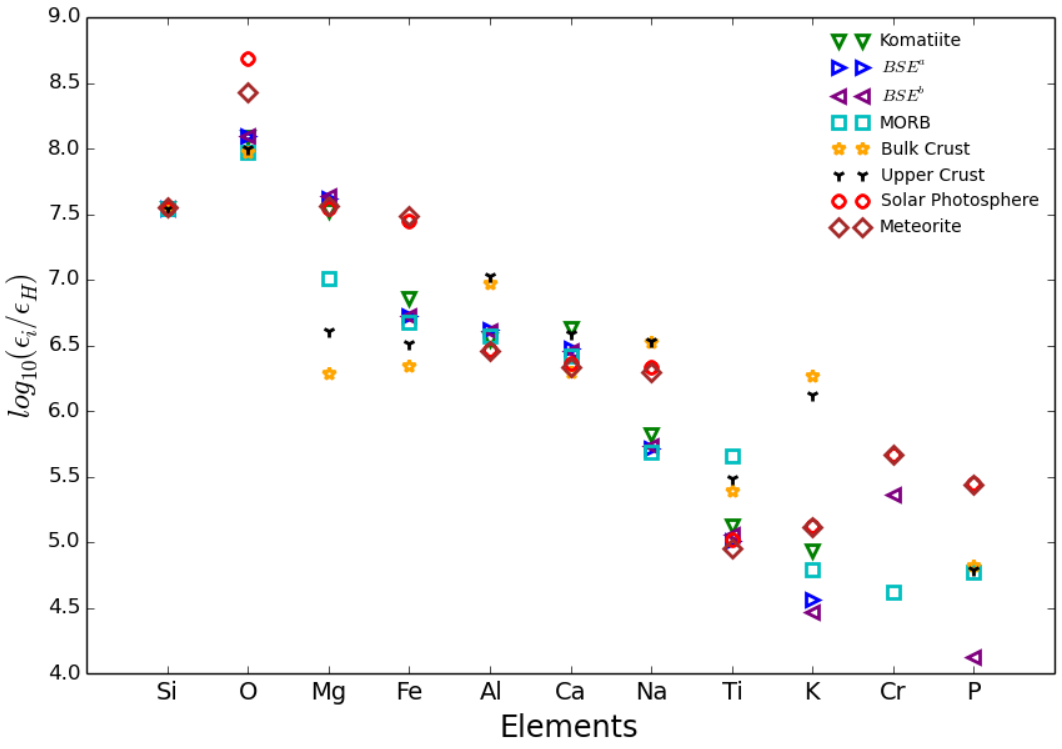

Figure 1: Abundance of various elements in the $\log_{10}(\epsilon_H) = 12$ scale, calculated from six rock and magma compositions found on earth. Komatiite and BSE^a compositions are used by Miguel et al. (2011a) and BSE^b, MORB, Bulk Crust and Upper Crust compositions are used by Ito et al. (2015) in their atmospheric models for evaporating planets. The solar photospheric and meteorites abundances of the same elements are also shown for comparison, values for which are obtained from Grevesse et al. (2007).

The abundances are also plotted in the log scale in the figure 1, which shows a comparision of all the six types of rocks in terms of their element content. The solar and the meteorite abundances are also shown in the figure for comparison. Si content is equal in every composition because of it being the reference element. Although this might vary in reality, the variation of Si is not significant even amongst Solar and Meteoritic compositions (Palme et al., 2013) and serves as a good first order approximation to analyze the differences of other elements taken into consideration. The O content is found to be approximately half a magnitude lower for each of the Earth silicates as compared to Solar composition. The amount of Mg found in BSE is nearly identical to Solar values but compositions such as MORB, UC and BC have significantly lower Mg content. The Fe content in all five compositions is lesser than Solar values. BC and UC have higher Al as compared to Solar. All of the Earth silicates have higher Ti content as compared to Solar. Finally the amount of K is found to be greatly varying amongst the silicates with BC and UC compositions having almost 20

times higher content as compared with BSE.

3 Equilibrium chemistry

We assume the atmospheric processes to be driven by equilibrium chemistry in local thermal equilibrium (LTE). Chemical equilibrium means that the local gas-phase chemical composition depends only on the local temperature, pressure and elements abundance (Madhusudhan et al., 2016). The relative element abundances are calculated with respect to a specified temperature, by minimizing the gibbs free energy of the system. The total pressure of the system is a summation of the individual partial pressures of chemical species that are in a state of chemical equilibrium.

The equilibrium chemistry stays valid only in the regimes where chemical reactions are fast enough to be the dominating mechanism. This is the case for atmospheres of cool stars and brown dwarfs, where chemical equilibrium has been most commonly applied (Tsuji, 1973; Fegley Jr and Lodders, 1996; Allard and Hauschildt, 1996; Helling et al., 2008). Equilibrium chemistry has also been applied to exoplanets that are hot-enough $\sim$ 2000 K, such as by Moses et al. (2011); Venot et al. (2012); Lee et al. (2015). Dis-equilibrium processes such as photochemistry play an important role in the upper layers of the atmosphere but has been ignored in this work.

3.1 Equilibrium chemistry model

The gas-phase composition is derived assuming chemical and local thermal equilibrium (LTE). The chemical equilibrium code contains 14 elements(H, He, C, N, O, Si, Mg, Al, Fe, S, Na, K, Ti, Ca) and 158 primary molecular species resulting due to their combination. The equilibrium constants are fitted to the thermodynamical molecular data of the electronic version of the JANAF tables (chase 1986). Element conservation equations are provided as auxiliary conditions for the chemical equilibrium (Woitke and Helling, 2004). We apply a chemical equilibrium approach and use the code described in Bilger et al. (2013).

Table 3: Characteristics of the modelled planets. (All values are approximations of recent findings.)

Planets	a [AU]	T_{eff} [K]	M [M$\oplus$]	$\log_10$(g) [cm/s^2]	References
55 Cnc e	$\sim$0.015	2400	8.63	3.33	Demory et al. (2016)
HD149 026b	$\sim$0.042	$\sim$1800	114	3.23	Fortney et al. (2006)
CoRoT-7b	$\sim$0.017	2300	$<$9	$\sim$3.5	Schaefer and Fegley (2009a)

Hydrogen-rich chemistry: The previous studies on the atmospheres of Super-Earths have all assumed a volatile free atmosphere consisting of only the gases present after vaporization from the surface. It is highly possible for such a planet to have atmosphere consisting of the silicates vaporized from the mineral rocks on the surface and while one may argue that close-in planets face a fate similar to that of Mercury and undergo extensive atmosphere and mass loss, Super-Earths can retain their atmospheres even at such close proximity due to their deeper potential wells (Perez-Becker and Chiang, 2013; Rappaport et al., 2014). Replenishment of the grains in the atmosphere could also be achieved by condensation at cooler temperatures near the day-night terminator or at

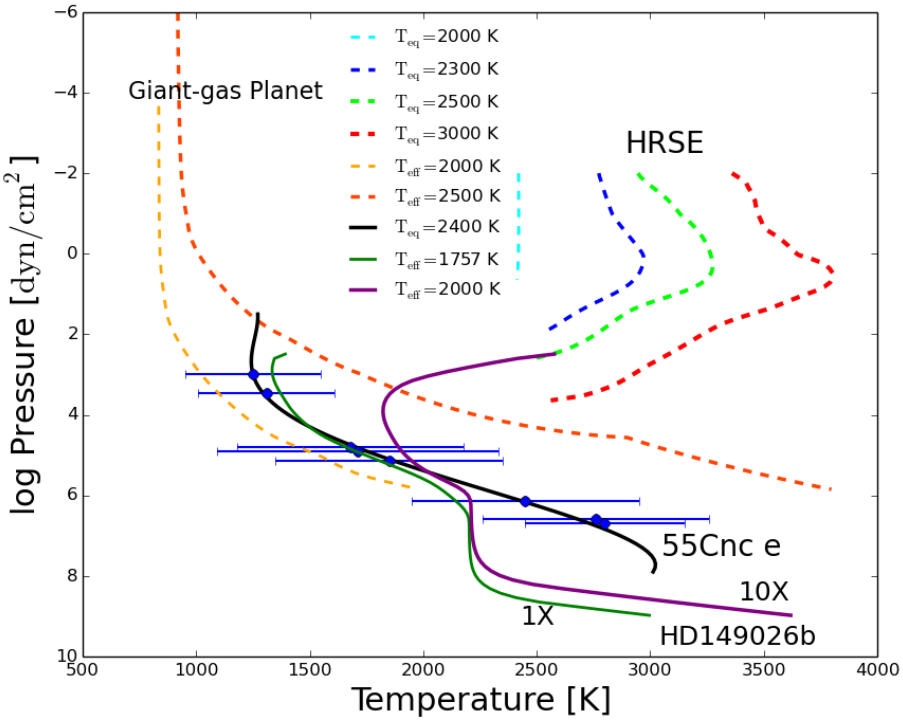

Figure 2: Shows the Temperature Vs. Pressure profiles of different objects considered for this study. The dashed lines correspond to simulated T vs. P profiles whereas the solid lines show the expected atmospheric profiles of discovered exo-planets. There are two giant gas atmosphere profiles in which the yellow profile has log(g)=5.0 and orange profile has log(g)=3.0. The T vs. P profiles corresponding to four Hot rocky Super-Earth(HRSE) are shown with increasing equilibrium temperatures which are derived from Ito et al. (2015). The green and purple profiles correspond to HD149026b are taken from Fortney et al. (2006) where "1X" and "10X" corresponds to profiles with Solar and 10 times the Solar abundances. The black solid line corresponds to the expected profile for 55 Cnc e taken from Demory et al. (2016) and the error bars are shown as well.

lower pressures (Schaefer and Fegley, 2009a; Castan and Menou, 2011). The existence of hot giant planets with a possibility of volatiles is suggested to be due to the migration of these objects from their initial accretion orbits closer to their parent star due to their gravitational interaction with the protoplanetary disk or other perturbations influenced by the objects nearby (see Madhusudhan et al. (2014)).

These giant planets or super-Earths retain their volatile gas reserve while being close to their stars and its intense radiation. Hence, it is highly likely that these planets will have a chemistry consisting of the volatiles combined with the gases vaporized from the solid surface due to a very high temperature. Given sufficient time, the atmosphere will be highly enriched with gases escaped from the surface and hence the abundances comparable to the abundance of the surface. We chose two possible scenarios for our analysis i.e a H-rich chemistry for a young object around its star and another case with significantly reduced-H possibly due to atmosphere blow out or Jeans escape.

3.2 Inputs

The code takes the local gas temperature(T) and pressure(P) structure as an input where in it determines the partial pressure and number densities of each species for every local total-pressure as a function of the temperature. It also takes the initial set of element abundances which represent the abundances in the lowest layers of the atmosphere assuming a well-mixed gas phase. It calculates the first ionization states in the gas-phase mixture. The T,P structure that we input into the code approximately models the 1-D local gas T,P resulting from the stellar irradiation at the sub-stellar point of the planets in the cases of CoRoT-7b, HD149026b, 55 Cnc e and is shown in the figure 2. Section 4, briefly describes the atmospheric processes used to model each of these celestial objects, which includes the radiative effects due to the stellar radiation. Our approach is to analyze the gas-phase compositions resulting from these converged T,P structures.

Element Abundances: The element abundances have been derived using the method described in section 2 and listed in the table 2. The values for all the other elements that are not listed in the table have been kept at solar abundance adopted from Grevesse et al. (2007). This includes the scenario of a Hydrogen-rich chemistry consisting of solar abundance for H, He, C. The low-H chemistry has been carried out with a H concentration of, $\mathbf{log(\epsilon_H) = 5.0}$.

4 Atmospheric composition of close-in Super Earths and giant gas planets

This section summarizes the atmospheric models and the resulting gas-phase compositions from the chemical equilibrium code. First we begin with the atmospheric structure of a giant gas planet adopted from Helling et al. (2008) to derive the initial gas-phase chemistry for a volatile-rich atmosphere which has high temperatures of upto T_{eff} = 3500 K. Then we move on to analyze the atmospheric compositions resulting from a theoretical model of HRSE used by Ito et al. (2015) similar to the possible atmospheric profiles of CoRoT-7b. We also study the compositions for a theoretical atmospheric model of 55 Cnc e which is adopted from that described by Demory et al. (2016). Finally we do a similar analysis on the atmospheric chemistry of HD149026b (Fortney et al., 2006) and study the differences in the resulting chemistry due to an increase in Solar abundance and also due to low Hydrogen in the atmosphere.

4.1 Giant gas planet atmosphere

A gas giant or hot Jupiter type planets atmosphere is composed primarily of volatile gases, and the temperature range can be 500 - 3000 K near the sub-stellar point Helling and Woitke (2006a). Local increase in opacity in the atmosphere might also lead to an increase (backwarming) or decrease of temperature. Figure 3 shows the atmospheric profiles of three different Hot Jupiters that are derived from the DRIFT-PHOENIX model atmosphere simulations Helling and Woitke (2006b). A 1D atmosphere model is determined by the effective temperature $T_{\rm eff}$, surface gravity log(g) and **element abundances** of the object. Observable total flux of the body, $F_{\rm tot} = \int F_\lambda d\lambda$ through the atmosphere is related to the $T_{\rm eff}$ as,

$$F_{\rm tot} = F_{\rm rad} + F_{\rm conv} = \sigma T_{\rm eff}^4. \quad (7)$$

where σ=Stefan-Boltzmann constant, the luminosity of the body is related to the total flux as,

$$L = 4\pi R^2 \sigma T_{\rm eff}^4. \quad (8)$$

where R= Radius of the object[cm].

The surface gravity is determined in terms of log(g) = log(GM/R^2) where G = Gravitational constant[$cm^3 g^{-1} s^{-2}$], M = Mass of the object[g].

The description of a Hot Jupiter atmosphere requires to model the local thermodynamic($T_{\rm gas}$ vs. $P_{\rm gas}$), hydrodynamic($v_{\rm gas}$ vs. $\rho_{\rm gas}$) and chemical properties($n_{\rm x}$, x -chemical species (ions, atoms, molecules, cloud particles)) which would be used to predict the observable quantities such as particular gases based on the measured radiative flux F_λ. The atmospheric model used in this study is in local thermal equilibrium(LTE) with an open boundary and radiative energy transport equations were used to determine the local gas temperature. Local gas pressure is calculated assuming hydrostatic equilibrium. The equations of state, opacity data and further chemistry close this system of equations (Helling and Casewell, 2014).

Results: We analyze the atmosphere of a Hot Jupiter with a starting BSE composition. We find the atmosphere to be dominated with volatile gases such as H_2, H, CO etc. Mg emerges as the primary abundant gas due to the silicate composition which is not the case with a solar composition as can be seen in the table 4. It is followed by C_2H_2, N_2, HCN, Fe and SiS which replaces H_2S as an abundant species due to increased Si abundance in the atmosphere. Other species such as Al, Ca,

Na, Si, SiO etc. also are found to be abundant which also contribute primarily to the dust cloud formations in the mineral dust cloud models used by Helling et al. (2008). The H_2O abundance decreases drastically for a BSE composition due to an increase in C/O ratio which results in the replacement of O with C molecules to form C_2H_2.

The first row of the Figures 6,7,8,9,10 show the resulting gas-phase compositions for the primary dust-forming species that are used in the cloud formation analysis. This analysis becomes important because the dominant species play a key role in the growth-reactions after the seed formations have taken place in the lower pressure regions of a planets atmosphere (Helling and Woitke, 2006a; Woitke and Helling, 2004). We find Si, SiH, SiO, SiN, Si2+, Si+ and SiO_2 as the most abundant Silicon species in gas-phase. SiO decreases in the concentration as compared to a solar composition due to an increase in the C/O ratio which results in fewer available O atoms for combining with Si and thus Si is the most abundant gas species for a BSE composition. For Ti species, Ti, TiC, TiS, TiO, Ti2+, TiO2 emerge to be primary species where the abundance of Ti is much higher as compared to the other species. This is also different from a solar composition as lower O results in lesser TiO and TiO2 formation. Similarly Fe is the primary gas-phase species followed by FeH, Fe+, FeS and FeO. Mg and Al follow a similar trend where Mg and Al atomic gases dominate the gas-phase followed by their hydrides. Metal enriched solar chemistry is shown in the panel 2 of the plots wherein the elements were enriched by a factor of 10 except H and He.

Table 4: List of 20 most abundant species in gas-phase compostions resulting from atmospheric equilibrium chemistry of 1. Gas Giant (T_{eff}=2500 K), 2. 55 Cnc e(T_{eq}=2400 K), 3. HD149026b(T_{eq}=1757K) and 4. CoRoT-7b(T_{eq}=2300 K), arranged according to their decreasing concentration in the atmosphere for Solar and BSE types of element abundances as listed in Table 2.

No.	Gas Giant		55Cnc e		HD149026b		CoRoT-7b	
	Solar	BSE	Solar	BSE	Solar	BSE	Solar	BSE
1.	H_2	H_2	H_2	H_2	H_2	H_2	H	H
2.	H	H	H	H	H	H	CO	CO
3.	CO	CO	CO	CO	CO	CO	O	C
4.	H_2O	Mg	H_2O	C_2H_2	H_2O	Mg	H_2	H_2
5.	Mg	C_2H_2	Mg	Mg	Mg	CH_4	Si	Si
6.	SiO	N_2	SiO	N_2	SiO	N_2	Fe	N
7.	N_2	HCN	N_2	SiS	N_2	C_2H_2	N	Mg
8.	Fe	Fe	Fe	HCN	Fe	SiO	S	N_2
9.	H_2S	SiS	H_2S	CH_4	H_2S	SiS	N_2	S
10.	Na	Al	Na	SiO	Na	HCN	Mg	Mg^+
11.	SiS	Ca	SiS	Fe	SiS	Fe	Mg^+	Na^+
12.	HS	Na	HS	Al	CaH	Na	Fe^+	Fe
13.	AlOH	Si	AlOH	Na	AlOH	Al	Al^+	Cl
14.	S	SiO	Al	Ca	HS	Ca	Na^+	O
15.	Ca	Ti	CaH	Si	Al	Si	Ca^+	Al
16.	CO_2	CH_4	K	SiH	MgH	SiH	SiO	Ti^+
17.	Al	SiC_2	S	AlH	K	CH_3	Si^+	CN
18.	K	$CaCl_2$	TiO	Si_2C	AlH	MgH	Cl	K^+
19.	S_2	SiH	MgH	CH_3	Al_2O	$CaCl_2$	C	CS
20.	TiO_2	K	MgOH	Ti	TiO	Ti	K^+	Ca

4.2 Atmospheres of Hot Super-Earths (CoRoT-7b)

Schaefer and Fegley (2009a) presented the possible compositions of the "silicate atmosphere" that is in gas-melt equilibrium with the molten rocky surface with no highly volatile elements such as H, C, N, S, and Cl (i.e., volatile-free magma ocean). They considered temperatures, T, of 1500–3000K and gravity of $logg \approx 3.5$, which corresponded to the planetary properties for CoRoT-7b, and assumed several compositions for the volatile- free magma, including the Earth's continental and oceanic crusts, the bulk silicate Earth (BSE), and the bulk silicate moon. We use converged T,P profiles with similar planetary properties as CoRoT-7b previously used by Ito et al. (2015) in their work for theoretical spectra for such rocky planets. The simulated atmosphere used by Ito et al. (2015) which is shown in figure 3, is a 1D plane-parallel thermal structure which is in radiative, hydrostatic and chemical equilibrium. They use the method developed by Toon et al. (1989) to calculate the T,P where they integrate the so-called two-stream equations with the assumption of quasi-isotropic radiation, adopting the δ-Eddington approximation. The radiative equilibrium

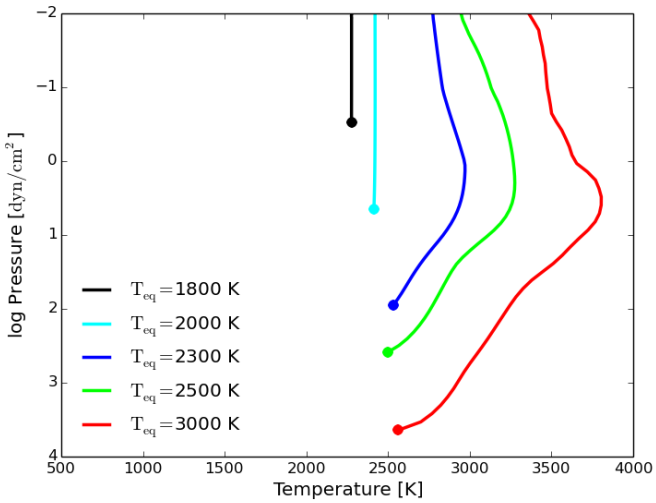

Figure 3: Thoretical T_{eq} vs. log P_{eq} for five types of HRSE models with increasing T_{eq}. These profiles are adopted from Ito et al. (2015). The circles at the end of the profiles show the temperatures near the surface of the rocky Super-Earth.

condition is given by $\int_0^\infty F_{net,\nu} d\nu = F_o$, where F_o is the constant flux. The ground pressure, P_g and molar fraction x_A are the functions of the ground temperature T_g which is determined as per the net radiative flux equation 7, assuming the magma ocean is a blackbody. The sub-stellar point equilibrium temperature is given as,

$$T_{eq}^4 = (1 - A_P)\frac{R_*^2}{D^2}T_*^4, \tag{9}$$

where R_* and T_* are respectively, the radius and temperature of the host star, A_P is the planetary albedo, and D is the orbital distance of the planet. The host star is assumed to emit blackbody radiation of 6000 K and the magma composition is assumed to be BSE.

In the temperature profiles shown in the figure 3, thermal inversion is seen in the cases of $T_{eq} \geq 2300$ K. The absorption of the incident stellar radiation is stronger compared to the planets internal radiation, which results in thermal inversion for P $\geq 10^{-5}$ bars. The absorption occurs due to the presence of SiO, Na and K where SiO absorbs in the UV whereas Na and K absorb in the visible frequencies. In the cases of $T_{eq} \leq 2000$ K, the atmosphere is isothermal due to the fact that the atmosphere is so optically thin that the ground is directly heated by the stellar irradiation (Ito et al., 2015). Although a comparison for the gas phase composition is attempted, there are some differences in the fitting of the gas-phase compositions into the T,P profiles. We set our initial element abundance as volatile-rich chemistry to derive an initial estimate of the possible atmosphere provided such planet is able to retain its primordial volatile atmosphere. The feedback of introduction of volatile gases would certainly be significant including an increased atmosphere scale height due to dominant atoms of lighter species but the effects have been ignored in this work.

Results: Figure 4 shows the gas-phase compositions resulting from four different types of rock compositions as listed in the Table 2. It should be noted that our gas-phase chemistry has Hydrogen

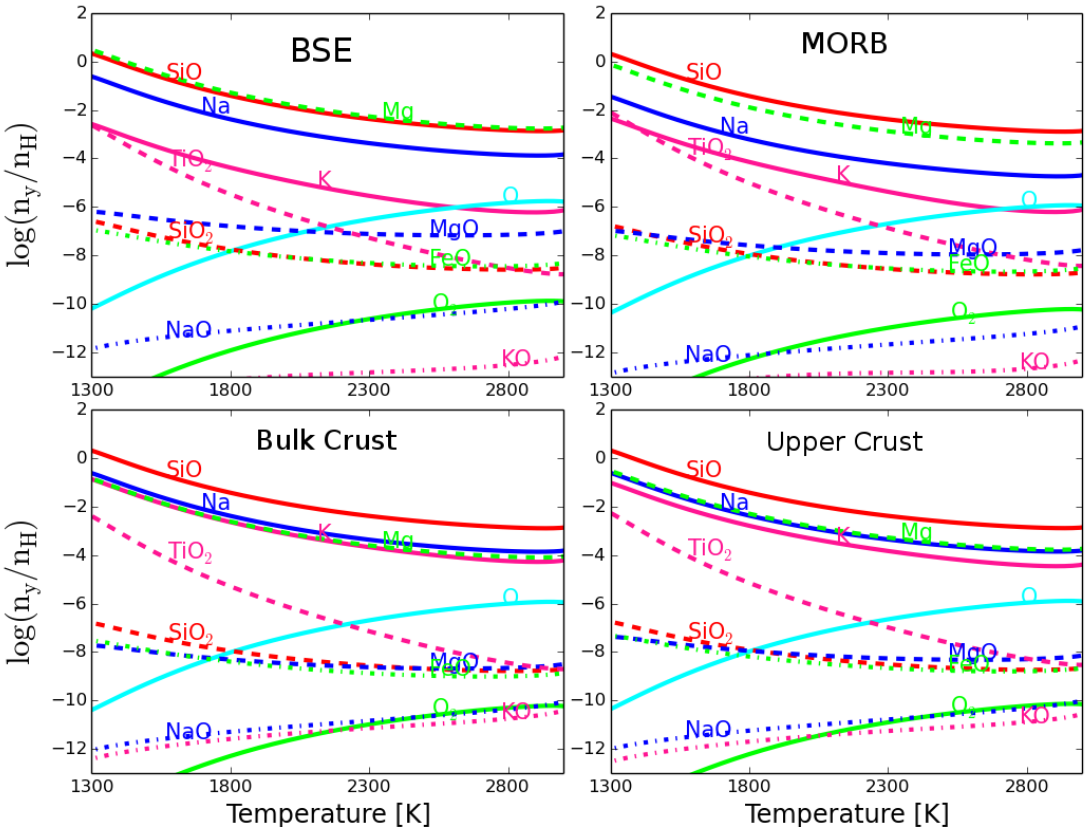

Figure 4: Gas-phase compositions in relative abundance with respect to Hyodrogen for four types of possible rock compositions for a HRSE type of atmospheric profile.

as its dominating species which can be better compared to a volatile-rich planet with a Earth-like rocky core which when exposed to the extreme irradiation from it's parent star would have it's surface in the semi-molten/molten state. We have analyzed the silicates to study their abundances and draw a comparison with previous studies such as that of Schaefer and Fegley (2009a); Miguel et al. (2011a); Ito et al. (2015) and we assume that the surface in and around the sub-stellar point of the planet has been hot enough to allow for the vaporization of surface which would mean all the elements present in the rock are enriched in the atmosphere with the same abundances.

It can be seen that except Upper Crust, all the other types of compositions produce an almost identical gas-phase composition where the highest constituents emerge to be Mg, SiO, Na, ,Fe, K, O irrespective of the type of rock abundance used. In the case of Upper Crust, the amount of Na, K and SiO decreases with an increase in temperature but the overall abundance is much lesser than the other compositions. This result is in contrast with the results found by Schaefer and Fegley (2009a); Miguel et al. (2011a); Ito et al. (2015) wherein they find the most abundant species to be Na. This difference is due to the difference in deriving atmospheric compositions. We assume all the elements to be present in the atmosphere in similar abundances with respect to that in

the surface where as they calculate their gas-phase compositions such that the element abundance changes with increasing temperatures. Schaefer and Fegley (2004) use the method of *fractional vaporization* of silicates to derive their total pressures. A fractional vaporization of 0% would mean that no gases has escaped the atmosphere where as a fractional vaporization of 50% would mean half of the initial planetary atmosphere has been lost. This process differs from the model of Bilger et al. (2013) which uses the total pressure from the hydrogen dominated atmospheric gas species.

4.3 Possible atmosphere on 55 Cnc e

55 Cnc e is an interesting candidate to study the potential atmospheric compositions due to its mass and radius estimated at 8.09 ± 0.26 $M_\oplus$ (Nelson et al., 2014) and 2.17 ± 0.10 $R_\oplus$ (Gillon et al., 2012) which makes is fall under the category of a Super-Earth. Given the extremely high equillibrium temperature of $T_{eq} \sim 2400$ K and it's proximity to the parent star, it is highly likely that the planetary lithosphere is weak and most of the day-side surface of the planet will be in a semi-molten or molten state which would lead to magma oceans and possibly volcanic activity on the irradiated day-side (Demory et al., 2016).

55 Cnc is the brightest star which has a transiting exoplanet 55 Cnc e enabling it to be measured in exquisite detail in the visible as well as Spitzer 4.5 μm IRAC Photometric band (Demory et al., 2012; Winn et al., 2011; Gillon et al., 2012). Based on the precise measurement of mass and radius alone Demory et al. (2011) suggested a silicate-rich interior with a dense H_2O envelope of 20% by mass, Gillon et al. (2012) suggested a purely silicate planet with no envelope, Madhusudhan (2012) suggested a carbon-rich planet with no envelope, Demory et al. (2016) suggested an atmospheric model in which multiple volcanic plumes explain the large observed temperature variations on the dayside. The T vs. P profile that we have taken into our study is derived from a sample T,P of Demory et al. (2016) which was retrieved based on the observed IRAC 4.5-μm brightness temperature (T_B) between $T_{min} = 1273^{-348K}_{+271K}$ and $T_{max} = 2816^{-368K}_{+358K}$. It is important to note that such a planetary atmosphere would mostly have isothermal profiles at the two extremes of the atmosphere given in terms of optical depth. The low optical depths would have surface temperature whereas the higher optical depths will have diffusive approximation (Demory et al., 2016).

Results: Figure 5 shows a comparison of the preliminary gas-phase concentration with respect to n_H derived for a solar and BSE element abundance using the sample T,P profile. The species shown are from Ti, Si, Mg, Fe, Al which show the potential dust forming species in gas-phase. The atomic species dominate the gas-phase in case of all the elements with BSE composition which is due to a higher C/O ratio as compared with solar. Tsiaras et al. (2015) in their analysis of an atmosphere around 55 Cnc e, show that the abundances of HCN and C_2H_2 increase many fold while the abundance of H_2O decreases drastically which is similar to the results that we obtain for a BSE composition as compared to a solar abundance, as can be seen in the table 4.

4.4 The atmosphere on HD149026b

HD 149026b is an extrasolar giant planet (EGP) with an orbit of 2.87 days around a metal-rich G0IV parent star. It has a radius of only $0.725R_J \pm 0.05R_J$ and a mass of $0.36M_J \pm 0.03M_J$ (114 $M_\oplus$) Sato et al. (2005). Evolution models suggest that the planet should have larger radii (Guillot et al., 1996), but it is decidedly small. Fortney et al. (2006) investigated the atmosphere models for the planet and find that the atmosphere will have a temperature inversion structure driven by the absorption of stellar flux by TiO and VO.

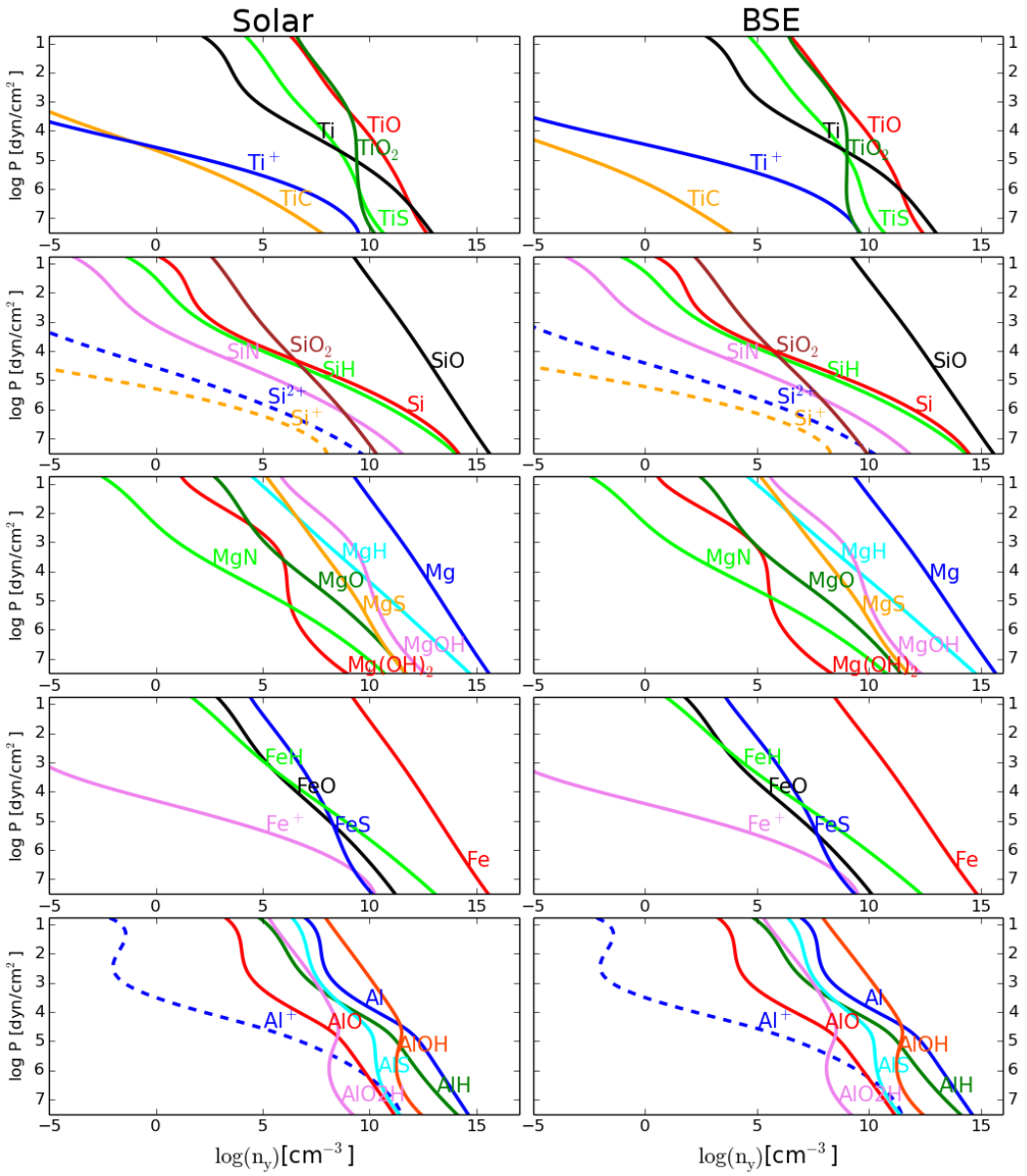

Figure 5: Shows the gas-phase compositions of some dominant species such as Ti, Si, Mg, Fe, Al resulting from a Solar (left) and a BSE (right) composition in a model atmosphere for 55 Cnc e. The chosen molecules/atoms/ions were found to be in higher concentrations.

The atmospheric T,P profiles used by us were obtained from Fortney et al. (2006). They used a plane-parallel model atmosphere code which uses the radiative-transfer scheme developed by Toon

et al. (1989). The profiles used in this work are shown in figure 2, where 1X corresponds to Solar abundance and 10X corresponds to a 10 times metal enriched atmospheric profile. We make the corresponding changes in our chemical equilibrium code to have a fair analysis of the resulting gas-phase compositions.

Results: Table 4 shows the overall abundant species which is very simialar to the results outlined for a Brown Dwarf. The temperature inversion is seen at around 2700 K where all the gases go through a sudden increase in concentration with decrease in height from above. The second panel of the third row for the figures show the plots for an enriched atmosphere with 10X the solar metallicity. The temperature profile changes drastically due to this enrichment which also leads to the temperature being maintained between 2000 K and 2500 K due to the additional absorption of stellar flux by TiO and VO. Third row of the figures 6, 7, 8, 9, 10 show the dominant gas-phase species for five elements. The abundance of oxides of Ti, Al, Fe, Mg and Si is higher for HD149026b as compared to other planets which would add to the cloud opacity and will contribute to higher dust cloud growth.

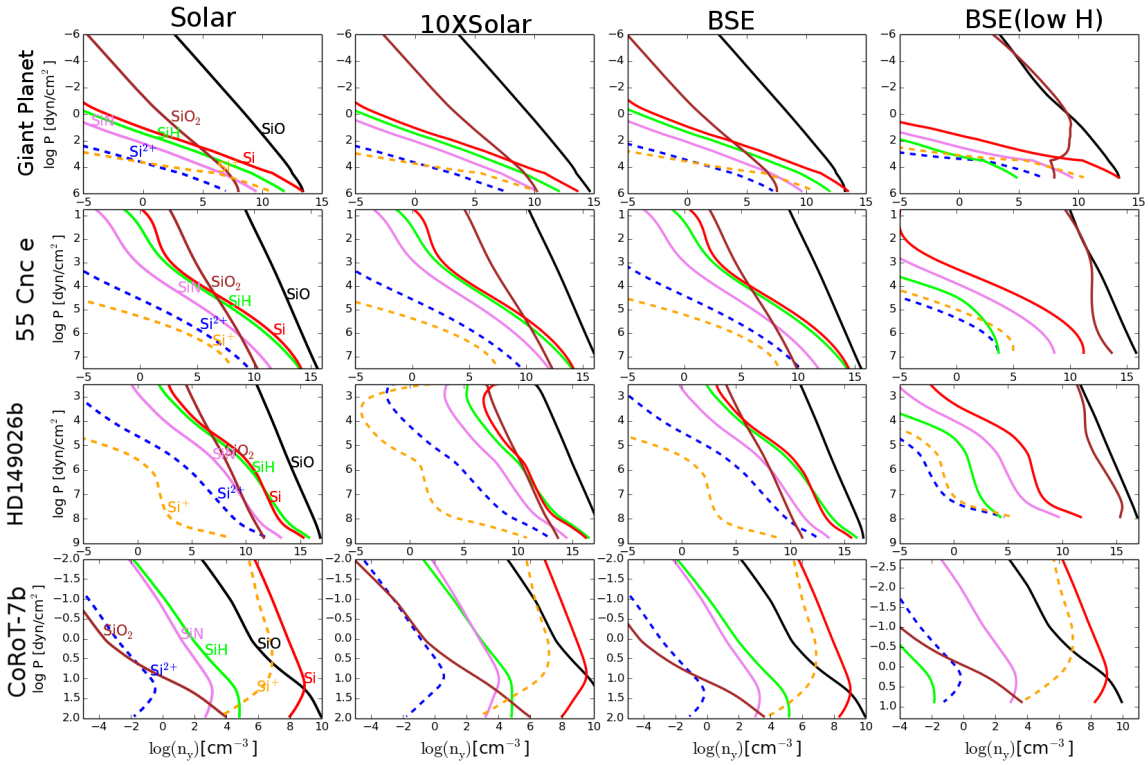

Figure 6: log Concentration, $n_y[cm^{-3}]$ vs. log Pressure [dyn/cm^2] plot for Silicate species resulting from equilibrium chemistry for four types of elements abundances and four different T,P profiles. "10XSolar" means an enrichment in the metallicity by a factor of 10 as compared to Solar Abundance. BSE(low H) has a BSE type of abundance with Hydrogen reduced to log H =5. The temperature ranges vary with respect to the type of atmosphere T,P as shown in the figure 2.

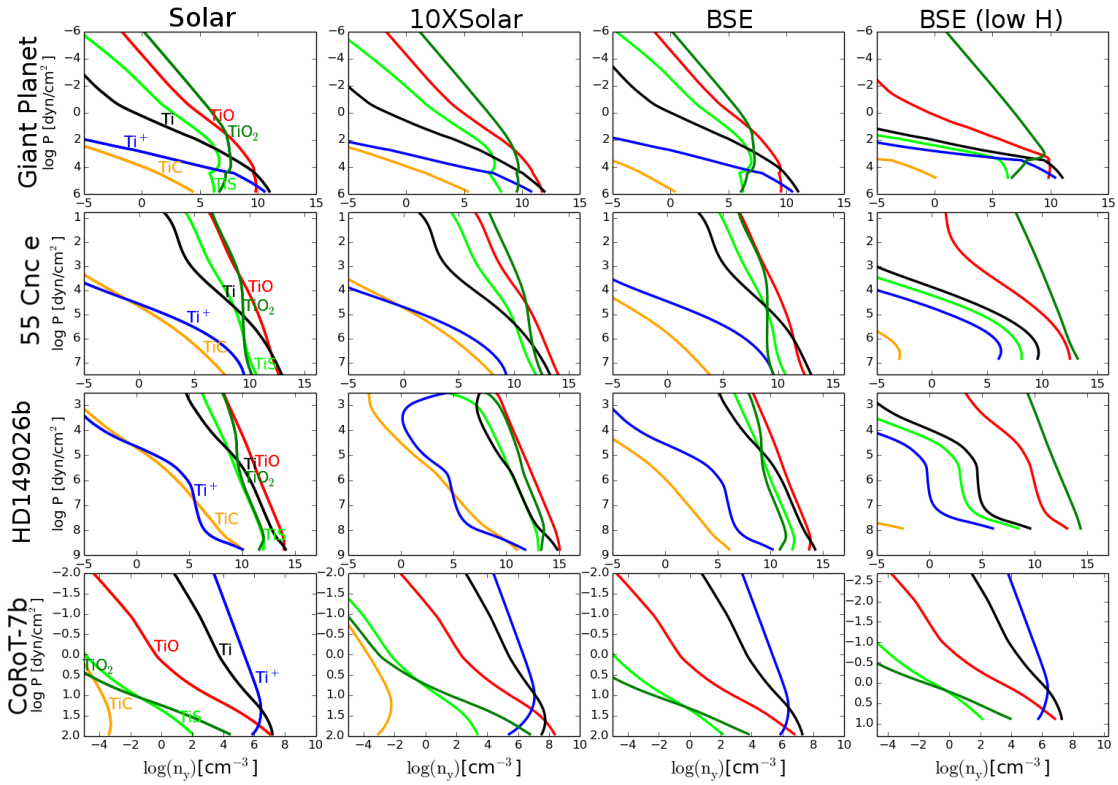

Figure 7: log Concentration, $n_y[cm^{-3}]$ vs. log Pressure [dyn/cm^2] plot for "Ti" species resulting from equilibrium chemistry for four types of elements abundances and four different T,P profiles. "10XSolar" means an enrichment in the metallicity by a factor of 10 as compared to Solar Abundance. BSE(low H) has a BSE type of abundance with Hydrogen reduced to log H =5. The temperature ranges vary with respect to the type of atmosphere T,P as shown in the figure 2.

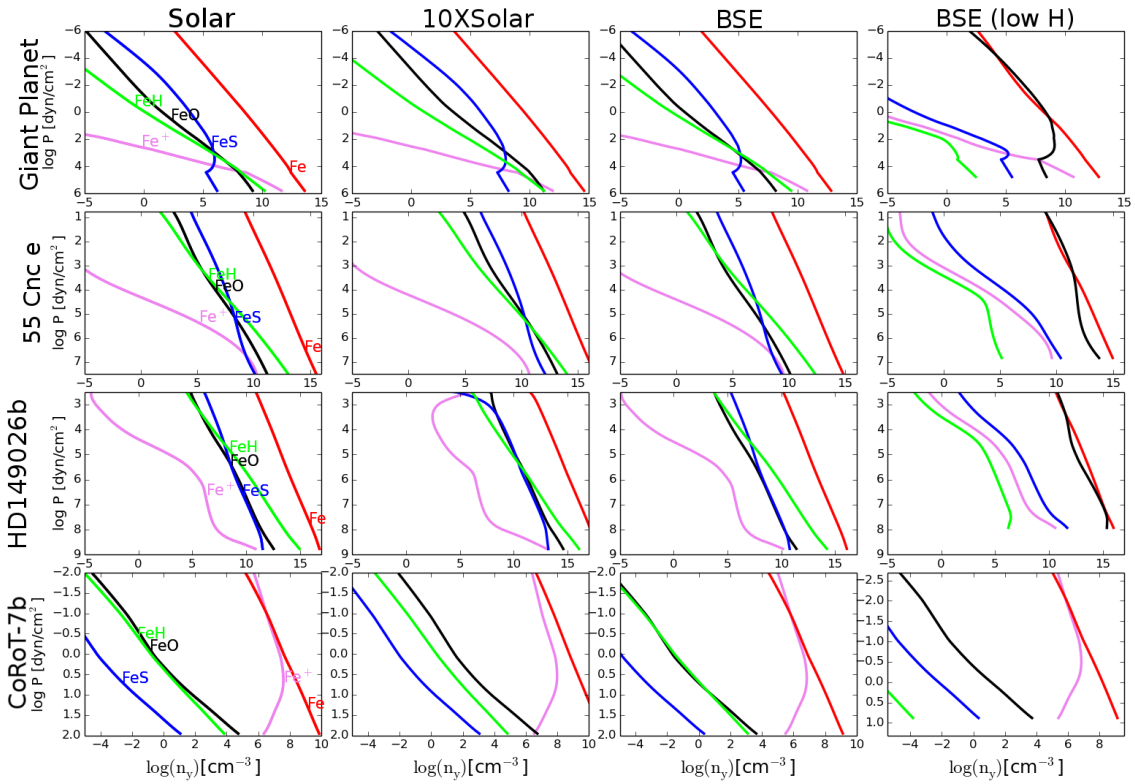

Figure 8: log Concentration, $n_y[cm^{-3}]$ vs. log Pressure [dyn/cm^2] plot for "Fe" species resulting from equilibrium chemistry for four types of elements abundances and four different T,P profiles. "10XSolar" means an enrichment in the metallicity by a factor of 10 as compared to Solar Abundance. BSE(low H) has a BSE type of abundance with Hydrogen reduced to log H =5. The temperature ranges vary with respect to the type of atmosphere T,P as shown in the figure 2.

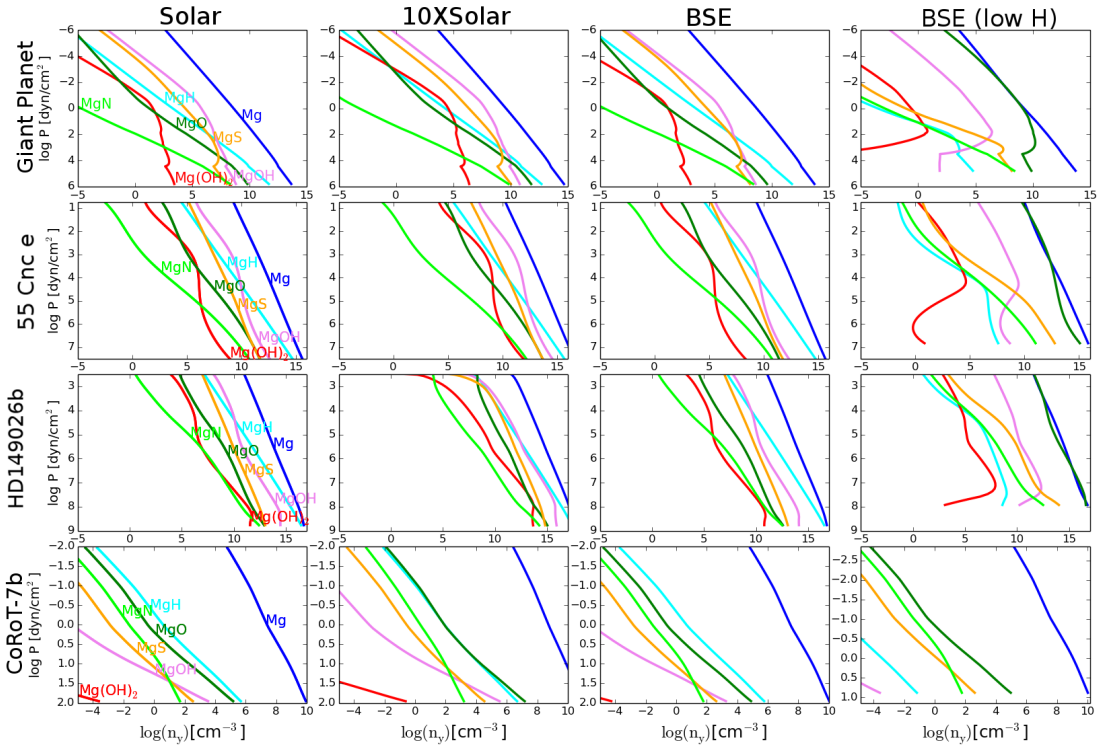

Figure 9: log Concentration, $n_y[cm^{-3}]$ vs. log Pressure [dyn/cm^2] plot for "Mg" species resulting from equilibrium chemistry for four types of elements abundances and four different T,P profiles. "10XSolar" means an enrichment in the metallicity by a factor of 10 as compared to Solar Abundance. BSE(low H) has a BSE type of abundance with Hydrogen reduced to log H =5. The temperature ranges vary with respect to the type of atmosphere T,P as shown in the figure 2.

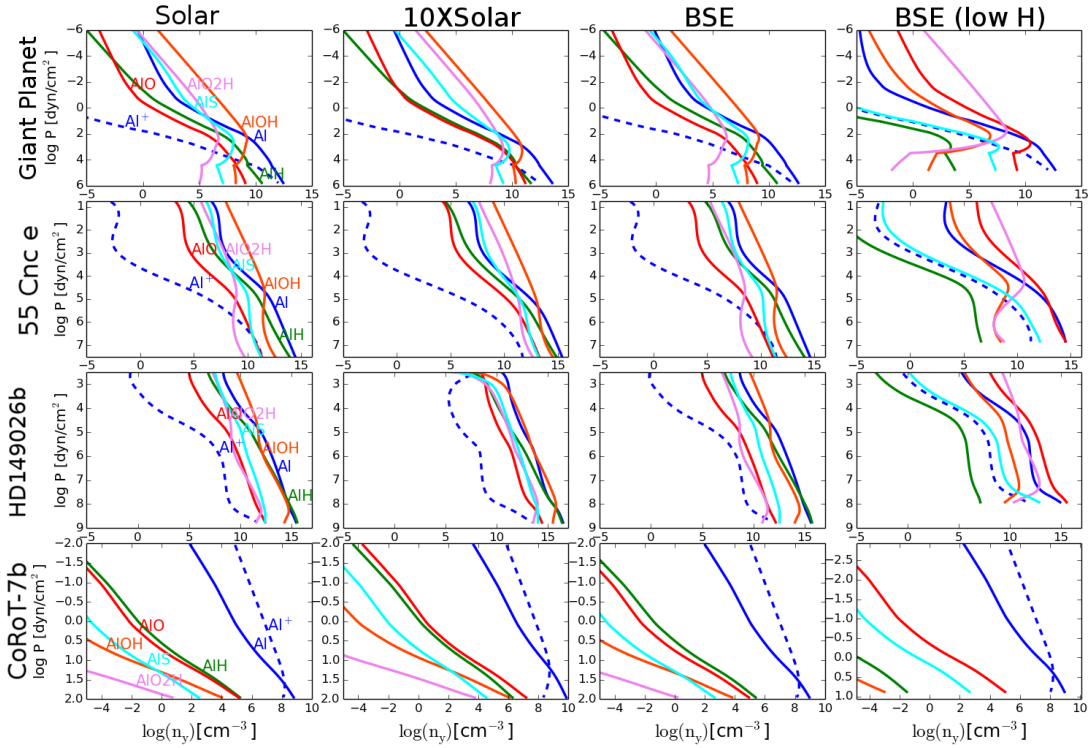

Figure 10: log Concentration, $n_y[cm^{-3}]$ vs. log Pressure [dyn/cm^2] plot for "Al" species resulting from equilibrium chemistry for four types of elements abundances and four different T,P profiles. "10XSolar" means an enrichment in the metallicity by a factor of 10 as compared to Solar Abundance. BSE(low H) has a BSE type of abundance with Hydrogen reduced to log H =5. The temperature ranges vary with respect to the type of atmosphere T,P as shown in the figure 2.

4.5 Summary: Atmosphere composition

Table 4 lists the most abundant gas-phase species resulting from the equilibrium chemistry with hydrogen dominated atmospheric compositions. We have analyzed the resulting chemistry for Solar and BSE types of element abundances. The primary abundant species is H_2 in all of our atmosphere's except that of CoRoT-7b which has atomic H as the dominating species due to its higher temperature and relatively thinner atmosphere similar to that of a HRSE. Our obtained results share similarity with the results obtained by Ito et al. (2015) and Miguel et al. (2011a) regarding the gas-phase silicate compositions. The BSE atmosphere for CoRoT-7b contains gases such as SiO, Mg, K, Na, O which are also found in the atmospheres of 55 Cnc e and HD149026b as shown in the table 4. Figures 6,7,8,9,10 show the gas-phase compositions of certain selected mineral species such as Si, Ti, Fe, Mg and Al for four types of planetary scenarios and four different compositions. SiO is the dominant gas resulting from Si in all of the planets cases except CoRoT-7b where we find Si to be dominant gas-phase species due to higher local gas temperature. It is followed by SiO_2 in the upper parts of the atmospheres for gas giant, 55 Cnc e and HD149026b. Atomic Fe is the dominant gas amongst the Fe gas-phase species, for all of the planets and compositions. Similarly atomic Mg is the dominant species amongst all of the Mg bearing gas-phase molecules, There is not much difference in the gas-phase compositions for Solar and BSE atmosphere which is due to our BSE C/O ratios being set at 0.5. Although the differences in silicate compositions such as BC, UC and MORB are quite big as compared to BSE and have been shown in the Figure 4. The panels labelled "10XSolar" have 10 times Solar metallicity. This does not change the resulting composition drastically but does lead to higher gas-phase concentrations of enriched elements as can be seen in the second column of Figures 6,7,8,9,10. It must be noted that our models do not take the feedback radiative transfer effects of the resulting gas-phase compositions due to increased metallicity. The feedback might result in localized thermal inversions due to certain gases. Fortney et al. (2006) in their gas-phase analysis for HD149 026b show inversion layers existing due to UV absorption by TiO and VO molecules.

We also analyze the effects of reduction of Hydrogen in each of the atmospheres. To study the effects of reduction in Hydrogen on the atmospheric chemistry, the element abundance of Hydrogen was reduced from $\log_{10}$H=12 to $\log_{10}$H=5. The abundances of other elements were kept unchanged and similar to a BSE composition. The last column of the figures 6,7,8,9,10 shows the resulting gas-phase chemistry of less Hydrogen in the four types of atmospheres as compared to the Hydrogen-rich chemistry. There is substantial increase in the amount of atomic Ti, Si, Mg, Fe, Al abundances in a less Hydrogen environment as compared to a Hydrogen dominant atmosphere. The abundance of hydrides such as SiH, MgH, FeH and AlH decreases drastically which is indicative of the loss of H atoms. The most noticiable difference that we see in a low-H environment is that the concentration of oxygen bearing molecules of all the selected elements increases being equal in abundance or replacing the atomic gases as the most dominant species. Gas-phase concentration of SiO_2, TiO_2, FeO and MgO increases in the atmospheres of gas giant, 55 Cnc e and HD149026b. In the case of CoRoT-7b we find the atomic species still quite dominant due to its higher local gas temperature.

5 Cloud formation on highly irradiated planets of non-solar composition

We analyzed the gas-phase compositions resulting from four different element abundances on four types of planetary atmospheres. Our analysis focused on the resulting gas-phase abundances of five most common silicate forming elements, Si, Ti, Mg, Fe and Al. Our gas-phase chemistry results indicate atmospheres enriched with mineral dust forming gaseous species such as SiO, SiO_2, MgH, Mg Fe, AlOH, Al. In this section we shall apply our understanding of the abundance of various gas-phase species to explore the possibility of dust cloud formations due to such mineral rich atmospheres. We follow the dust cloud modelling approach of Woitke and Helling (2003), Helling and Woitke (2006b), Helling et al. (2008) for hot atmospheres of brown dwarfs and giant gas planets and use the 1D kinetic cloud formation code DRIFT to perform detailed mineral cloud modelling on hot atmospheres of gas giant, HD149026b, 55 Cnc e and CoRoT-7b. The general properties of dust clouds such as nucleation rates, mixing timescales, grain sizes, grain compositions, dust-to-gas ratio and their variation along the vertical trajectory of cloud formation regime is discussed in this section.

5.1 Cloud formation process

The theoretical models for dust cloud formation and associated processes on Brown Dwarfs using the DRIFT model have been described in detail in Helling and Casewell (2014), Helling et al. (2008), Helling and Woitke (2006b). The cloud formation begins with the formation of seed particles from the pure gas-phase via homogeneous homomolecular nucleation of the TiO_2 gas in the upper rarified parts of the atmosphere. The nucleation rates, J_* are calculated in each of the case using Eq. (34) from Helling and Woitke (2006a), who use the modified classical nucleation theory of Gail et al. (1984). The equation used is given as,

$$J_*(t,r) = \frac{f(t,1)}{\tau_{gr}(1,N_*,t)} Z(N_*) \times exp\left((N_*-1)lnS(T) - \frac{\Delta G(N_*)}{RT}\right) \quad (10)$$

where f(1,t) is the number density of seed forming gas species, τ_{gr} is the growth timescale of the particle critical cluster size N_*, $Z(N_*)$ the Zeldovich factor, S(T) the supersaturation ratio and $\Delta G(N_*)$ the Gibbs energy of the critical cluster size.

Once the nucleation takes place, growth/evaporation of dirty mantles happens over these newly formed pure particles as per the models discussed in Woitke and Helling (2003), Helling and Woitke (2006a) and Helling et al. (2008) when a gas-phase species undergoes surface chemical reaction to form solid mantle over the particle. As is the case with the previously used Brown Dwarf models, we consider the reactions forming 12 different dust species (TiO2[s], Al2O3 [s], CaTiO3[s], Fe2O3[s], FeS[s], FeO[s], Fe[s], SiO[s], SiO2 [s], MgO[s], MgSiO3[s], Mg2SiO4 [s]) which react to form dirty grains with mantles of these species of various sizes dependent on the local gas density and temperature. The original DRIFT model used 60 growth reactions which contribute to the dust particle growth that has been used for the Brown Dwarf atmospheres. In this study we identify 19 additional growth reactions which can potentially contribute to the dust formation reactions which have been chosen primarily due to the higher concentration of the particular gas species in a silicate atmosphere. The growth reactions that were added to the original reactions listed in Helling et al. (2008) are listed below:

Table 5: Added surface reactions for the growth of dust particles. The solids resulting from these reactions are indicated with an [s] in the **rhs** of the reaction.

Reaction No.	Growth Reaction
1.	$2MgH + 2H_2O \longrightarrow 2MgO[s] + 3H_2$
2.	$2MgH + 2SiO + 4H_2O \longrightarrow 2MgSiO_3[s] + 5H_2$
3.	$MgH + SiH + 3H_2O \longrightarrow MgSiO_3[s] + 4H_2$
4.	$2MgH + 2SiN + 6H_2O \longrightarrow 2MgSiO_3[s] + 7H_2 + N_2$
5.	$MgS + Si + 3H_2O \longrightarrow MgSiO_3[s] + H_2S + 2H_2$
6.	$2MgN + 2Si + 3H_2O \longrightarrow 2MgSiO_3[s] + 3H_2 + N_2$
7.	$2MgH + SiO + 3H_2O \longrightarrow Mg_2SiO_4[s] + 4H_2$
8.	$4MgH + 2SiH + 8H_2O \longrightarrow 2Mg_2SiO_4[s] + 11H_2$
9.	$4MgH + 2SiN + 8H_2O \longrightarrow 2Mg_2SiO_4[s] + N_2 + 10H_2$
10.	$2MgS + Si + 4H_2O \longrightarrow Mg_2SiO_4[s] + 2H_2S + 2H_2$
11.	$2MgN + Si + 4H_2O \longrightarrow 2Mg_2SiO_4[s] + N_2 + 4H_2$
12.	$2SiH + 4H_2O \longrightarrow 2SiO_2[s] + 5H_2$
13.	$2SiN + 4H_2O \longrightarrow 2SiO_2[s] + N2 + 4H_2$
14.	$2SiH + 2H_2O \longrightarrow 2SiO[s] + 3H_2$
15.	$2SiN + 2H_2O \longrightarrow 2SiO[s] + N_2 + 2H_2$
16.	$2FeH + H_2 \longrightarrow 2Fe[s] + 2H_2$
17.	$2FeH + 2H_2O \longrightarrow 2FeO[s] + 3H_2$
18.	$2FeH + 2H_2O \longrightarrow 2FeS[s] + 3H_2$
19.	$2FeH + 3H_2O \longrightarrow Fe_2O_3[s] + 4H_2$

The grain growth is indicated by the growth velocities, χ_{net} cm/s. The growth velocity(χ_{net}[cm s^{-1}]) of the particle gives a measure of particle growth which can be stated as,

$$\chi^{net}(r) = (36\pi)^{-1/3} \sum_{s} \sum_{r=1}^{R} \frac{\Delta V_r n_r v_r^{rel} \alpha_r}{V_r^{key}} \left(1 - \frac{1}{S_r} \frac{1}{b_{surf}^{s}}\right). \tag{11}$$

where "r" is the index for the chemical surface reaction, ΔV_r the volume increment of the solid "s" by reaction r, n_r is the density of the gas-phase reactant particles, α_r the sticking coefficient of the reaction r, ν_r^{key} the stoichiometric factor of the key reactant in reaction r, v_r^{rel} relative thermal velocity of the gas species taking part in reaction r, S_r is the reaction supersaturation ratio and $1/b_{surf}^{s} = V_s/V_{tot}$ is the volume ratio of solid s. The evaporation is indicative with a negative particle growth velocity. The growth velocity is proportional to the gas particle density (n_d) which means that the growth velocity would increase as we go deeper into the atmosphere of each of the planets. It is also dependent on the relative thermal velocity of the reacting particles which means that some of the selected species would have higher growth rates than the others. DRIFT cloud model allows us to track the overall growth velocity of the solids formed over the TiO_2 seeds as well as the individual growth rates of 12 species selected to form the mantles over the seeds. The growth stops when the temperature is too high for the particles to sustain themselves and they evaporate. The individual growth of dust species is dependent on the local gas concentrations and efficiency of the chemical reactions.

Particle sizes increase with time due to growth reactions to form dirty grain mantles in the atmosphere. It begins soon after TiO_2 nucleation and continues until the particles become heavy enough and start to gravitationally settle after which they vaporize due to thermal instability. The particles encounter denser regions as they settle gravitationally and thereby also increasing their size in the process due to availability of more reaction material. The particles slow down as they fall deeper and achieve a terminal velocity before evaporating. Bigger dust particles would have a higher fall velocity and will eventually rainout faster. The mean grain radius ($< a >$) is stated as,

$$< a > (r) = \left(\frac{3}{4\pi}\right)^{-1/3} \frac{L_1(r)}{L_o(r)} \tag{12}$$

where L_o and L_1 are found by solving the dust moment equations as explained in Woitke and Helling (2003). Dust volume fraction (V_s/V_{tot} [%]) is an important parameter to study the evolution of dust as it falls deeper in the atmosphere. DRIFT allows to track the percentage of each of the 12 growth species reacting to form the dust particle after the nucleation at every layer of cloud forming region. TiO_2 volume fraction drops soon after the nucleation in the upper layers of the atmosphere. Growth reactions (condensation) starts happening soon after the nucleation provided the availability of sufficient gas-phase materials to react. The local dust number density (n_d) is stated as,

$$n_d(r) = \rho_{gas}(r) L_o(r) \tag{13}$$

where ρ_{gas}(r) is the local gas density of the reactant and L_o is the zeroth order of the dust moment equations explained in Woitke and Helling (2003).

5.2 Cloud model and Input Quantities

We use sample 1D atmosphere model profiles representative of a planets sub-stellar point to test the cloud formations resulting due to the various types of Earth compositions. We use the PHOENIX atmosphere model output(Helling and Casewell, 2014) for a giant gas planet with a T_{eff} of 2500K and surface gravity of log(g)=3.0 which has a local gas temperature ranging from 900 K to 3000 K. We perform the cloud formation simulations for 55 Cnc e which is a Super-Earth with a mass of **8.63** $\mathbf{M_\oplus}$ and HD 149026 b which is a semi-giant metal enriched planet with a mass of **116** $\mathbf{M_\oplus}$. The atmosphere profiles for 55 Cnc e is adopted from the preliminary atmospheric studies conducted by Demory et al. (2012). The atmosphere profile for the mineral rich HD149026b is adopted from the atmospheric modelling of Fortney et al. (2006). The C/O ratio at the start of the cloud formation process is fixed at **C/O=0.5** for all of the initial cloud formation cases so as to be able to discern the differences in the chemistry due to varying silicate compositions. All the other element abundances are varied according to the four types of Earth compositions that are Bulk Silicate Earth (BSE), Upper Crust (UC), Bulk Crust (BC) and Metal Oxide Rich Basalt (MORB).

Model setup and Input quantities: The inputs to the DRIFT cloud formation code for the planetary atmospheres takes the global T_{eff} and logg values for each of the planets. The atmosphere is divided into vertical layers each defined by its local T_{gas} and p_{gas}. The **surface gravity** values can be defined locally but has been kept constant which is equal to the global surface gravity value logg for this study for both of the planets. The **mean molecular weight** (μ) for both the atmospheres is set to be a constant at 1.364 g/mol calculated from the initial global element abundances. We have chosen the starting composition as Hydrogen-rich chemistry for this analysis with the element abundances changing from Solar to BSE, BC, MORB and UC compositions.

5.3 Atmospheric mixing

A vertical mixing mechanism is critical to sustain the clouds in the atmosphere lest the dust particles grow to a certain size and fallout thereby depleting the atmosphere off dust forming gas species preventing further cloud formation (Woitke and Helling, 2003). The vertical mixing is

parametrized using the eddy diffusion coefficient K_{zz}, which can be approximated as the strength with which material can be transported back into the atmosphere (Agúndez et al., 2014). There have been extensive research on the choice of K_{zz} for the cases of hot-Jupiters (Moses et al., 2011; Parmentier et al., 2013; Agúndez et al., 2014). Parmentier et al. (2013) use vertical diffusive coefficients determined by following passive tracers in their general circulation model (GCM). They adopt a K_{zz} (cm^2 s^{-1}) = 5×10^8 p $^{-0.5}$ bar for HD 209458 b which is a gas-giant. Agúndez et al. (2014) used K_{zz} (cm^2 s^{-1}) = 10^7 p$^{-0.65}$ (bar) for the case of HD 189733 b which is also a gas-giant. Miguel and Kaltenegger (2013) use constant values of K_{zz} (cm^2 s^{-1}) = 10^9 for their atmospheric models of Mini-Neptunes. The pressure dependence for the vertical mixing would be much more in the case of a gas-giant with large horizontal circulation winds driving the vertical transport of material (Agúndez et al., 2014), whereas in the cases of irradiated planets with very thin atmospheric cover, constant value of the diffusion coefficient is a good first order approximation.

We follow the procedure of diffusive vertical mixing described by Lee et al. (2015) for the vertical mixing of condensed gases into the atmosphere. Although they have applied turbulent diffusion by using the vertical velocity component (v_z) from their 3D RHD model, we use the vertical diffusion constant K_{zz} (cm^2 s^{-1}) which parametrizes the diffusive circulation as given by the equation 14.

$$K_{zz} = Hp(r).v_z(r) \tag{14}$$

where Hp(r) is the pressure scale-height of the planets atmosphere and v_z(r) is the vertical velocity as a function of radius (r).

The mixing timescale (τ_{mix}) for the convective velocity is given by Helling et al. (2008),

$$\tau_{mix} = const.\frac{Hp(r)}{v_{conv}(r)} \tag{15}$$

The v_{conv}(r) is approximated as v_z(r) and substituted in the equation 14 to obtain the diffusive mixing timescale as,

$$\tau_{mix} = const.\frac{Hp^2}{K_{zz}}. \tag{16}$$

We use equation 16 to model the recirculation of the gas species wherein we vary the parameter K_{zz} for every planet. The cloud formation is heavily dependent on the diffusive velocity constant and hence we vary it until a uniform cloud formation is achieved. A k_{zz} (cm^2 s^{-1}) = 10^{11} was chosen for the cloud formation on 55 Cnc e which was kept constant for every composition. It is important to point out that the cloud formation does not start below a K_{zz} value of 10^9 (cm^2 s^{-1}). This value of the eddy diffusion coefficient is moderately high and is also an indicator of the strength of vertical mixing required so as to achieve cloud formation via replenishment of lost minerals. The K_{zz} value for HD 149026 b is selected to be $\mathbf{10^{15}}$ $\mathbf{cm^2}$ $\mathbf{s^{-1}}$.

6 Cloud formation results

55 Cnc e: We use an arbitrary T,P profile for 55 Cnc e representative of the planets dayside as derived by Demory et al. (2016) from their Spitzer IRAC 4.5 μm observation for the planet. We use the Solar and Earth BSE, UC, BC, MORB compositions to investigate the possibility of a silicate atmosphere resulting in cloud formations. A vertical diffusive coefficient(K_{zz}) of 10^{13} cm^2s^{-1} was used for performing our cloud formation analysis. This value of K_{zz} has been kept constant for the whole of the vertical atmospheric re-circulation. It must be noted that our adopted value for K_{zz} is significantly high for a global replenishment, although Lee et al. (2015) have shown in their 3D modelling for HD 189733b which is a giant gas planet, local K_{zz} values to be reaching as high as 10^{12} cm^2s^{-1}.

Figures 13 and 14 show the dust cloud properties for 55 Cnc e. The TiO_2 nucleation takes place at $\sim 10^{1.2}$ dyn/cm^2 in the upper atmosphere of 55 Cnc e. The cloud formation takes place in a thin region of the atmosphere where the local gas temperature and densities favour particle growth. J_* differs slightly (by an order of magnitude) for the various compositions with MORB composition attaining the highest nucleation rates which can be attributed to its higher abundance of Ti molecules leading to efficient nucleation. The growth rates are also observed to be the highest due to an abundance of available material to condense on the existing seeds which makes the particles grow rapidly as soon as the nucleation happens. The particle growth happens until roughly $\sim 10^{3.6}$ dyn/cm^2. The growth rates are the highest for a solar composition followed by BSE, BC, UC and MORB. The particles encounter denser regions as they settle gravitationally and thereby also increasing their size in the process due to availability of more reaction material. In the case of 55 Cnc e, we observe a uniformity in the dust constituents which is due to the fact that the cloud layer is thin as compared to the cloud layer in the gas giant as evident from the atmospheric pressure range of cloud formation in Figure 13. The Solar and BSE compositions have Mg silicates (∼25%) for the major part of the dust cloud and it further increases to ∼30% of the dust before evaporation. Si growth species SiO and SiO_2 constitute ∼15% of the dust. Fe, Al and Ca species are present in minority (<5%) in BSE atmosphere. SiO and SiO_2 form the majority of the dust particles for BC, UC and MORB atmospheres which is due to lower Mg content available to condense on the dust particles. Also, the cloud base which is situated at $\sim 10^{3.6}$ dyn/cm^2 is predominantly composed of Si dust species.

HD149 026 b: HD149 026 b can be classified as a semi-giant planet with a mass of 114 $M_\oplus$. Fortney et al. (2006) investigate the atmospheric and cloud properties for the planet with varying metallicities such as [M/H] of 1x , 3x , 10x with TiO and VO enrichments for 3x and 10x. We perform our cloud modelling on a similar T,P profile for 1x Solar abundance as shown in the figure 2 while varying the silicate abundances according to our four different Earth Silicate compositions of BSE, BC, MORB and UC. Figure 15 shows the cloud properties due to a solar composition and 16 shows the differences in the cloud properties due to the variations in element abundances. Our models suggest a high value of vertical diffusive constant, K_{zz} of 10^{13} cm^2s^{-1} or higher is needed for the atmosphere to be able to form dust clouds.

Figures 15 and 16 show the dust cloud properties for HD149 026b. The cloud formation after TiO_2 nucleation for HD149 026 b begins at $\sim 10^{2.5}$ dyn/cm^2. There is relatively large differences

in the nucleation rates(J^*) values with a MORB composition having the highest nucleation due to its higher Ti abundance (refer to fig. 1). The particle growth velocities are the highest for a Solar composition because of which the particles reach the highest sizes(~ 3 μm) for a Solar composition followed by a BSE composition. The drift velocities ($< V_{dr} >$) are found to be in the same sequence of Solar followed by BSE, MORB, BC and UC respectively. The particles formed due to a solar composition are sustained for a larger range of pressure before they evaporate completely at $\sim 10^{5.2}$ dyn/cm^2. The dust number densities (nd) are the highest for a MORB composition again due to its higher Ti content which allows more seed particles to form on them. We can expect an atmosphere modelled with 10x Ti content, similar to Fortney et al. (2006) to have proportionally higher dust number densities which would be indicative of higher dust opacities. The particle growth happens until roughly $\sim 10^{4.5}$ dyn/cm^2. A Solar and BSE composition in HD149026b follows a similar trend of dust composition wherein, just after the nucleation, Mg silicates dominate the dust volume fraction with $\sim$40% of the dust having Mg dust species and is followed by Si($\sim$40%) and Fe($\sim$30%) species which dominate the cloud base region. For BC, UC and MORB compositions, our models suggest dust particles majorly being formed out of Si species $\sim$ 60 % and the cloud base having an increased amount of Al_2O_3[s] which goes upto $\sim$40% at the cloud base. Table 6 shows the average volume fractions for each of the dust forming species on the three of the possible atmospheres. Although our dust cloud model uses the T,P profiles obtained by Fortney et al. (2006) for their atmosphere analysis, our model does not take the feedback of cloud formation into account. Fortney et al. (2006) consider atmospheric inversions due to the presence of TiO in their models but our dust cloud models suggest an upper atmosphere in which TiO is heavily depleted due to the seed formations. This would result in a loss of temperature inversion or suppression of the inversion zone to lower parts of the atmosphere where the TiO density increases slightly.

CoRoT-7b: CoRoT-7b is an interesting candidate to analyze the possibility of cloud formation due its extremely high local gas temperatures (>2500 K) and low local gas densities (-2 $< \rho_{gas} <$ 2 [dyn/cm^2]) making it a challenging candidate for dust cloud formations. Models for silicate atmospheres by Schaefer and Fegley (2009a) predict clouds of Na and K forming around the planet. They also state the possibility of silicate clouds which would condense and rain out there by depleting those minerals from the gas-phase or there also would be a possibility of circulation of the minerals to the night side and getting deposited, again thereby depleting the warmer parts of the elements. The only possibilities of sustained dust clouds arise only if the vertical replenishment occurs on the day-side due to strong vertical winds driving the condensed minerals into the gas-phase. We investigated the possibility of cloud formation on sample atmosphere profiles resembling a rocky planet such as CoRoT-7b with four different T_{eff} values as shown in the figure 2. The atmosphere profile is representative of the sub-stellar point of the planet. K_{zz} was varied between values ranging from 10^7 cm^{2}s^{-1} to 10^{15} cm^{2}s^{-1} but our solutions indicate no successful dust cloud formations at the sub-stellar point, most likely reason being the extremely high local gas temperatures which doesn't allow the nucleation and growth reactions to take place. Fig. 17 shows the results from the attempted cloud formation code on CoRoT-7b.

7 Discussions and Summary

In this work we have studied the effects of changing atmospheric parameters such as local gas pressure, temperature and varying element abundance to analyze the impact on resulting equilibrium gas-phase chemical compositions and also to study the changes in dust cloud properties due to these. We identify four different Earth crust compositions such as BSE, BC, UC and MORB following the works of Schaefer and Fegley (2009a), Miguel et al. (2011a) and Ito et al. (2015) who modelled the possible atmospheric formations due to vaporization of Silicate magma. The weight oxides(%) for the various silicates were converted into Hydrogen scale element abundances using a conversion method similar to that applied in the case of Meteorites. The obtained element abundances were used as inputs to the atmospheric and cloud formation models. Although the works of Miguel et al. (2011a) and Ito et al. (2015) assume a completely volatile free atmosphere, we model the atmospheres consisting dominantly of volatiles with the heavier elements enriched to equal the Earth silicate atmospheric compositions. Four different planetary scenarios have been adopted to study the possibility of cloud formations due to silicate compositions and the effects of different atmospheric conditions on dust particle properties have been analyzed. We use an atmospheric equilibrium chemistry code which assumes local thermal equilibrium (LTE) conditions and performs Gibbs free energy minimization to derive the atmospheric chemical compositions as outlined in Bilger et al. (2013).

Our equilibrium chemistry gas-phase composition results reflects the adopted silicate compositions. Apart from the volatile rich atmosphere consisting primarily of H_2 H and CO, there is an increase in content of gases such as Mg, Fe, SiS, Al, Ca, Si, Ti and K which can be directly linked to the adopted silicate compositions and the differences with respect to Solar composition are outlined in the Table 4. We find that the overall sequence of gas-phase concentrations in such high temperature atmospheres follow a similar pattern with different planetary objects such as gas giant, CoRoT-7b, 55 Cnc e and HD 149026b. Only the local gas-phase concentrations differ depending upon the local gas temperature and pressure. Although the gas-phase results obtained for a model HRSE (CoRoT-7b) atmosphere is different due to its extremely high local temperature and its low density atmosphere which makes most of the species exist in their ion or atomic states. The atmospheric composition is also found to be heavily dependent on the C/O ratios. An almost Solar C/O of 0.5 results in an increase in the H_2O content whereas a C/O $\sim$ 1 results in an increase of species such as HCN, C_2H_2 and CH_4 in the atmospheres due to excess availability of C which leads to new stable molecule formations.

Table 6: Dust volume fractions (V_s/V_{tot} [%]) in percentages for individual growth species, Maximum nucleation rates and particle sizes contributing to the dust formation in three types of compositions. We show the cloud properties in three different stages of its evolution i.e. at cloud Top (where TiO_2 nucleation begins), at the middle (approximate half-length of the cloud) and at the cloud Base (where the dust species evaporate).

Vol. Fractions[%]	**Comp.**	**Brown Dwarf**			**55Cnc e**			**HD149026b**		
		Cloud Top	Middle	Base	Cloud Top	Middle	Base	Cloud Top	Middle	Base
Pressure[dyn/cm^2]		$10^{-5.5}$	$10^{1.3}$	10^{3}	$10^{1.1}$	$10^{2.5}$	$10^{3.65}$	$10^{2.5}$	10^{3}	$10^{5.2}$
TiO_2[s]	Solar	100.0	0.04	1.66	0.4	0.1	5.05	99.6	2.2	1
	BSE	100.0	0.1	4.47	1.67	0.13	6.4	99.9	4.61	2.2
	BulkCrust	100.0	0.3	5.8	29	0.9	9.9	99.9	45.2	3.02
Al_2O_3[s]	Solar	0	2.79	97.4	0.7	1.07	3.9	0.002	0.8	13.4
	BSE	0	6	94.2	0.9	1.35	6.13	<0.001	1.2	17
	BulkCrust	0	17.7	93.1	3.6	6.3	16	<0.01	6.7	45
$CaTiO_3$[s]	Solar	0	0.15	0.47	0.01	0.01	0.35	<0.001	0.05	1.1
	BSE	0	0.16	1	0.03	0.05	0.35	0	0.07	1.0
	BulkCrust	0	0.7	0.7	0.13	0.16	0.96	0	0.4	2.6
Fe_2O_3[s]	Solar	<0.001	<0.001	<0.001	5.15	6	<0.001	<0.001	<0.001	0
	BSE	0	0	0	0.3	0.33	0	0	0	0
	BulkCrust	0	0	0	0.08	0.14	0	0	0	0
FeS[s]	Solar	0	0.08	<0.01	4.8	8.02	0.2	0.01	1.4	0.1
	BSE	0	0.05	4.2	1.7	2	0.1	<0.001	0.15	0.04
	BulkCrust	0	<0.01	0	1.36	1.86	0.02	0	0.04	<0.01
FeO[s]	Solar	0	<0.01	<0.01	5.6	5.6	0.2	0.01	0.5	0.05
	BSE	0	0	<0.001	1.11	1.25	0.02	<0.001	0.01	<0.01
	BulkCrust	0	0	0	0.85	1.16	<0.01	0	<0.01	<0.01
Fe[s]	Solar	0	14.6	0.34	3.3	3.3	18.1	0.01	4	41.7
	BSE	0	4.11	0.14	0.6	0.7	4	0	0.8	9.5
	BulkCrust	0	2.2	0.05	0.5	0.7	1.9	0	0.8	4.2
SiO[s]	Solar	0	9.7	0.08	12.4	11.7	46.4	0.05	15	28
	BSE	0	45.9	0.16	13.4	13.4	66.4	<0.001	16.2	60.1
	BulkCrust	0	72.3	0.16	25	36.6	69.8	<0.01	35.6	44.5
SiO_2[s]	Solar	0	14.8	<0.001	14	13.2	3.5	0.05	15.7	2.8
	BSE	0	1.01	<0.001	15.1	15	2.32	<0.01	10.0	2.0
	BulkCrust	0	3.14	<0.01	28.08	41.1	0.8	<0.01	7.4	0.5
MgO[s]	Solar	0	5.1	<0.001	9.1	8.35	10.5	0.03	11	6.1
	BSE	0	15.8	<0.001	12.3	12.5	9	<0.01	10.5	5.0
	BulkCrust	0	0.6	<0.01	1.07	1.05	0.18	0	0.5	0.07
$MgSiO_3$[s]	Solar	0	22.4	<0.001	23.1	23.1	3.2	0.07	24.16	2
	BSE	0	6.05	0	22.4	22.7	1.9	<0.01	22.1	1.3
	BulkCrust	0	0.6	0	6.0	5.9	<0.01	<0.01	1.0	<0.01
Mg_2SiO_4[s]	Solar	0	30.2	<0.001	21.3	19.4	8.3	0.07	25.4	3.6
	BSE	0	20.7	0	30.1	30.3	3.3	<0.01	34.1	1.6
	BulkCrust	0	2.2	0	4.17	4.1	0.13	<0.01	2.06	0.05
Max Nucleation Rates										
$\log_{10}J^*$ [cm^{-3}s^{-1}]	Solar		-8.1			12.13			5.98	
	BSE		-9.75			11.86			4.42	
	BulkCrust		-8.91			12.35			4.74	
Particle Sizes										
<a> [μm]	Solar	0.0019	0.033	0.55	0.008	0.012	0.002	0.0019	0.005	0.02
	BSE	0.0019	0.030	1.085	0.005	0.011	0.005	0.0019	0.004	0.008
	BulkCrust	0.0019	0.037	0.75	0.002	0.006	0.004	0.0019	0.002	0.005

The studied atmospheric compositions were used to analyze the possibility of cloud formations due to certain specific chemical species which could contribute to the dust growth reactions. The dust cloud calculations are performed using the DRIFT model developed by Woitke and Helling (2003), Helling et al. (2008) for minerals clouds modelling of giant gas planets and brown dwarfs. Our results indicate possible cloud formations on the model atmospheres of 55 Cnc

e and HD149 026b. The atmosphere profile for 55 Cnc e is adopted from Demory et al. (2016) and HD149026b is adopted from Fortney et al. (2006). This work is the first attempt at modelling the cloud formations on these planets due to Earth silicates. We have fixed the C/O ratios for this preliminary study to C/O = 0.5 in all the cases. Diffusive vertical mixing mechanism has been adopted following Lee et al. (2015) so as to enable element replenishment in the atmosphere. We find that the values at which cloud formation sets in is quite high ($> 10^{11} cm^2 s^{-1}$) for a global vertical recirculation indicating a requirement for strong vertical diffusion for dust clouds to be able to form. The possibility of high vertical replenishment mechanisms have not been explored in detail in this work but a large day-night temperature gradient may favour a circulation mechanism and hence increase the likeliness of dust clouds at or near the sub-stellar point. An atmosphere with no strong vertical recirculation would render the gas-phase mineral free after the dust formation which would precipitate clearing the heavier elements. Lee et al. (2015) suggest the removal of the dust forming minerals from the atmosphere would result in flattening of the spectral signatures from these elements and their associated molecules. Recent spectroscopic observations of 55 Cnc e by Tsiaras et al. (2015) suggest an atmosphere which has a high C/O $\sim$ 1 having a high concentration of HCN molecule. A Carbon rich atmosphere might lead to C as nucleation species rather than TiO_2 as used in our cloud models. Despite this recent observational finding, the dust cloud model for 55 Cnc e indicate particles to primarily consist of Mg silicates ($\sim$25%), followed by Si and a minor percentage of Fe, Al and Ca.

Our dust cloud models show great variation in particle sizes and compositions for different planetary scenarios. The particle sizes are found to be the largest in the case of giant gas planet which is indicative of the denser atmosphere resulting in more condensing material availability. The particle sizes follow the order of Gas Giant > HD149 026b > 55 Cnc e, with the largest particles found at the cloud base in each of the cases before the particle loses material and evaporate. The biggest particle sizes are $\sim$ 1 μm for Gas giant, $\sim$ 0.01 μm for 55 Cnc e, $\sim$0.02μm for HD149 026b. The particle number densities (nd/cm^3) are found to be 10 times higher for the atmosphere of 55 Cnc e as compared to HD149 026b which might contribute to higher cloud opacity on 55 Cnc e. The cloud thickness can be estimated by the range of dust formation regime on each atmosphere. The cloud thickness is maximum for gas giant spanning from $10^{-5.5}...10^{3}$ dyn/cm^2, followed by HD149 026b with pressure range of $10^{2.5}...10^{5.2}$ dyn/cm^2 and the thinnest cloud layer is formed on the super-Earth 55 Cnc e with a pressure range of $10^{1.1}...10^{3.6}$ dyn/cm^2.

We observe a similarity in the cloud property trend due to the changes in element abundances on each of the planets cases where cloud formation happens. The particle sizes are found to be maximum with a Solar and BSE composition for each of the planets. This is due to higher Mg and O content in the atmosphere with these abundances which results in higher dust growth due to species such as $MgSiO_3$[s] and Mg_2SiO_4[s]. The dust number density (nd) is found to be the highest for a MORB atmosphere which can be explained due to higher Ti content which results in more seed species formation during the nucleation stage. The particle composition also follows a similar trend due to changes in element abundances. Dusts in BC, UC and MORB atmosphere predominantly constitute of SiO and SiO_2 species and their percentages vary proportionally with the changes in element abundances. Similarly a BSE and Solar atmosphere would have dust particles predominantly of Mg_2SiO_4[s], $MgSiO_3$[s] and MgO[s]. Only the atmosphere of gas giant has pressures and temperatures suitable for cloud base to form particles of Al_2O_3[s] and Fe[s] species. Lee et al. (2015) in their analysis for 3D cloud formations on HD189 733b find similar high volume fractions of Fe and Al dust particles and suggest a locally lower cloud opacity due to Al_2O_3 and high opacity due to Fe particles which could alter the radiation propagation.

To summarize the results obtained in this work:
- Our models suggest possibility of mineral dust cloud formations on 55 Cnc e and HD149 026b. The atmosphere of CoRoT-7b or HRSE is found to be too warm for gas condensation to happen.
- Our results indicate that changes in silicate compositions result in significant changes in the compositions of dust particles.
- Solar and BSE atmospheres consists majorly of Mg dust species whereas BC, UC and MORB atmospheres consist of Si and Fe dust species.
- The dust properties for different compositions follow a trend of variation independent of local gas-phase pressures and temperatures. As an example, an atmosphere with high Ti content such as that found in MORB composition will have higher dust number density as compared to BSE, BC and UC compositions due to higher Ti seed particle formations.
- The atmospheres of 55 Cnc e and HD149 026b requires strong vertical replenishment mechanism to be able to sustain dust clouds. An atmosphere with no vertical replenishment would most likely result in the heavy minerals raining out, rendering the atmosphere free of heavy elements. This would result in flattening of the observed spectra caused due to these heavy minerals.

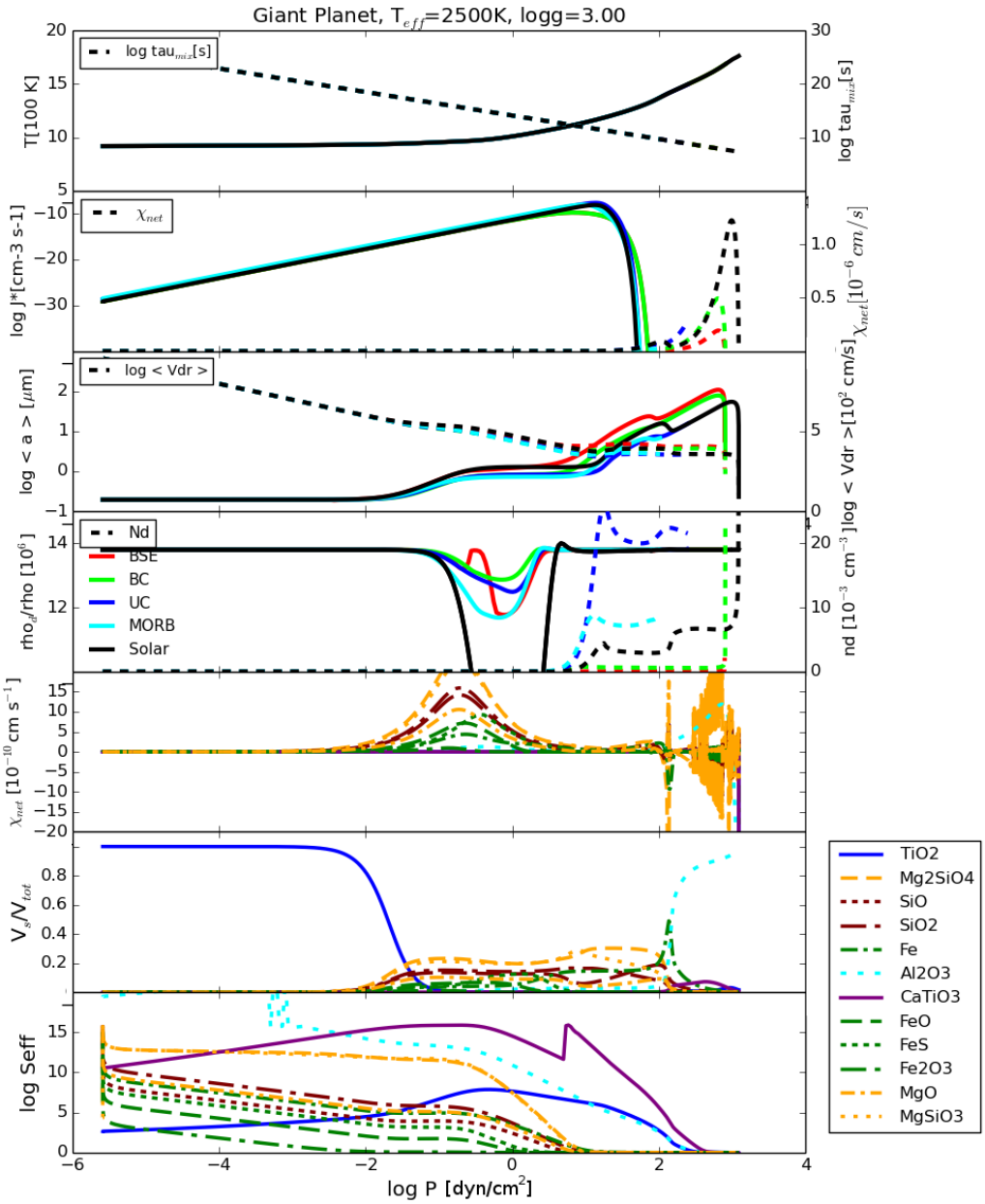

Figure 11: Showing the DRIFT cloud model results for Giant Planet (T$_{eff}$=2500K, logg=3.0) atmosphere with varying compositions. **1st Panel:** local gas temperature, T$_{gas}$[K] (solid), mixing time scale τ_{mix}[s] (dashed); **2nd Panel:** Nucleation rate, log J* (solid), dust growth rate χ_{net}; **3rd Panel:** Particle size, log $< a >$ [μm], Drift Velocity, log $< Vdr >$ [cm/s]; **4th Panel:** Dust density fraction, rho$_d$/rho, Particle number density, [cm^{-3}]. The cloud properties for five types of compositions are shown for each of the panels, Solar(Black), BSE(Red), Bulk Crust(Green), Upper Crust(Blue), MORB(Sky Blue). **5th Panel:** Individual grain growth velocity, χ_s [cm s^{-1}]; **6th Panel:** Material volume fraction, V$_s$/V$_{tot}$ [%]; **7th Panel:** Effective supersaturation ratio, log Seff.

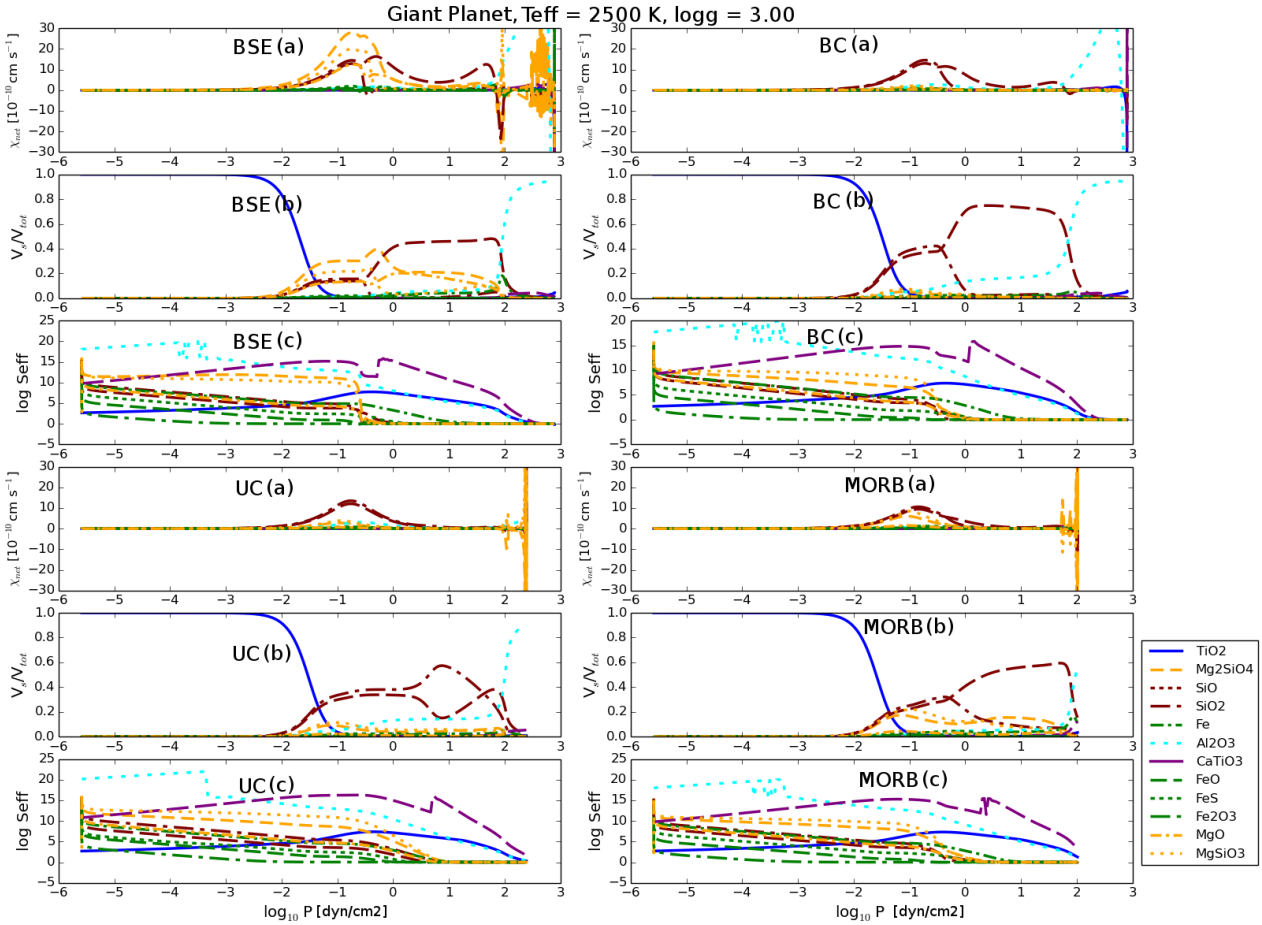

Figure 12: Showing the dust grain properties resulting from cloud formations on a hot Giant Planet (T_{eff}=2500K, logg=3.0) atmosphere for four different compositions. **(a)** Individual grain growth velocity, χ_s [cm s^{-1}]; **(b)** Material volume fraction, V_s/V_{tot} [%]; **(c)** Effective supersaturation ratio, log Seff. The four compositions BSE, BC, UC, MORB have been labelled on each plot.

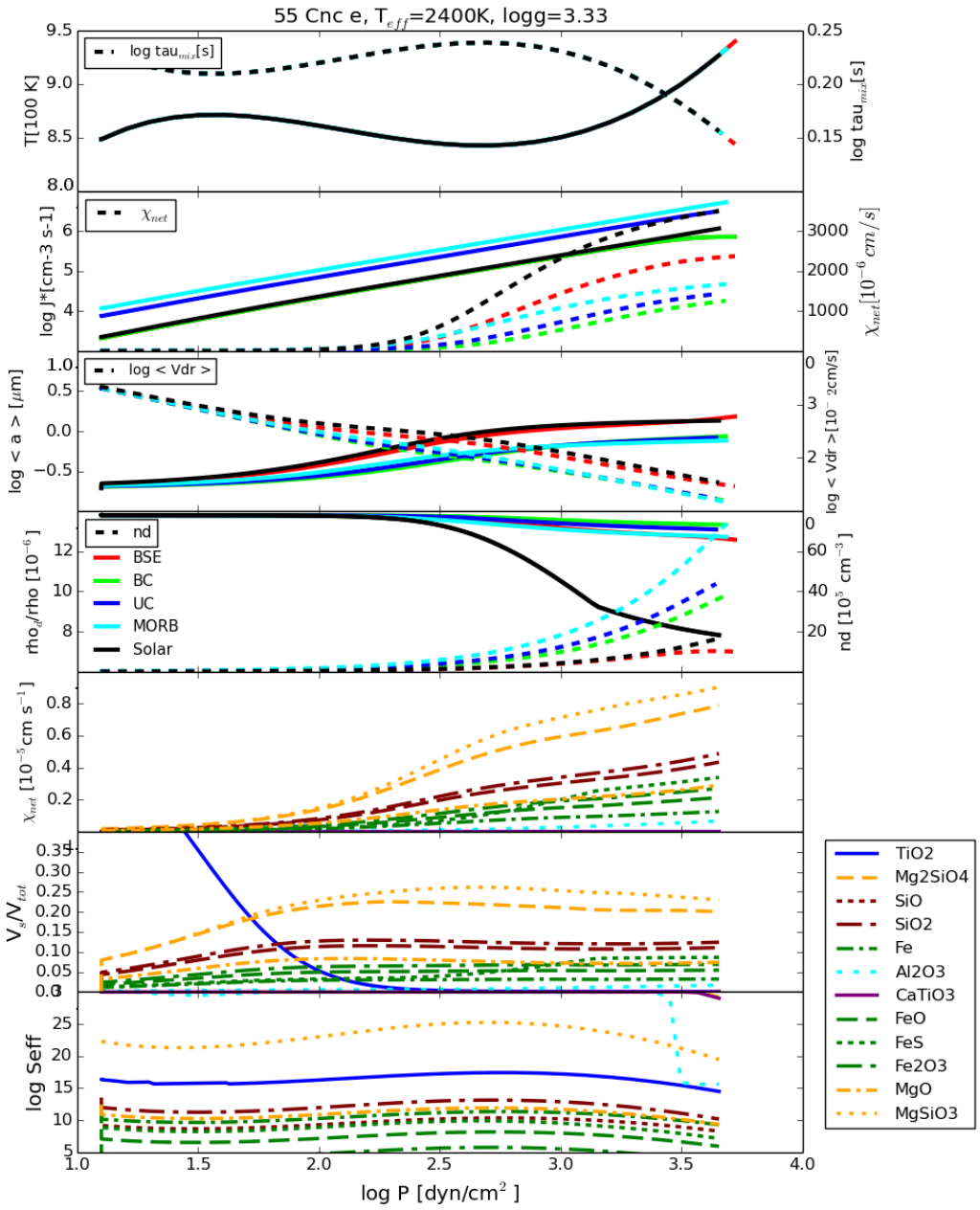

Figure 13: Showing the DRIFT cloud model results for 55Cnc e (T$_{eff}$=2400K,logg=3.33) atmosphere with varying compositions. **1st Panel:** local gas temperature, T$_{gas}$[K] (solid), Diffusive mixing time scale τ_{mix}[s] (dashed); **2nd Panel:** Nucleation rate, log J* (solid), dust growth rate χ_{net}; **3rd Panel:** Particle size, log $< a >$ [μm], Drift Velocity, log $< Vdr >$ [cm/s]; **4th Panel:** Dust density fraction, rho$_d$/rho, Particle number density, [cm^{-3}]. The cloud properties for five types of compositions are shown for each of the panels, Solar(Black), BSE(Red), Bulk Crust(Green), Upper Crust(Blue), MORB(Sky Blue). **5th Panel:** Individual grain growth velocity, χ_s [cm s^{-1}]; **6th Panel:** Material volume fraction, V$_s$/V$_{tot}$ [%]; **7th Panel:** Effective supersaturation ratio, log Seff.

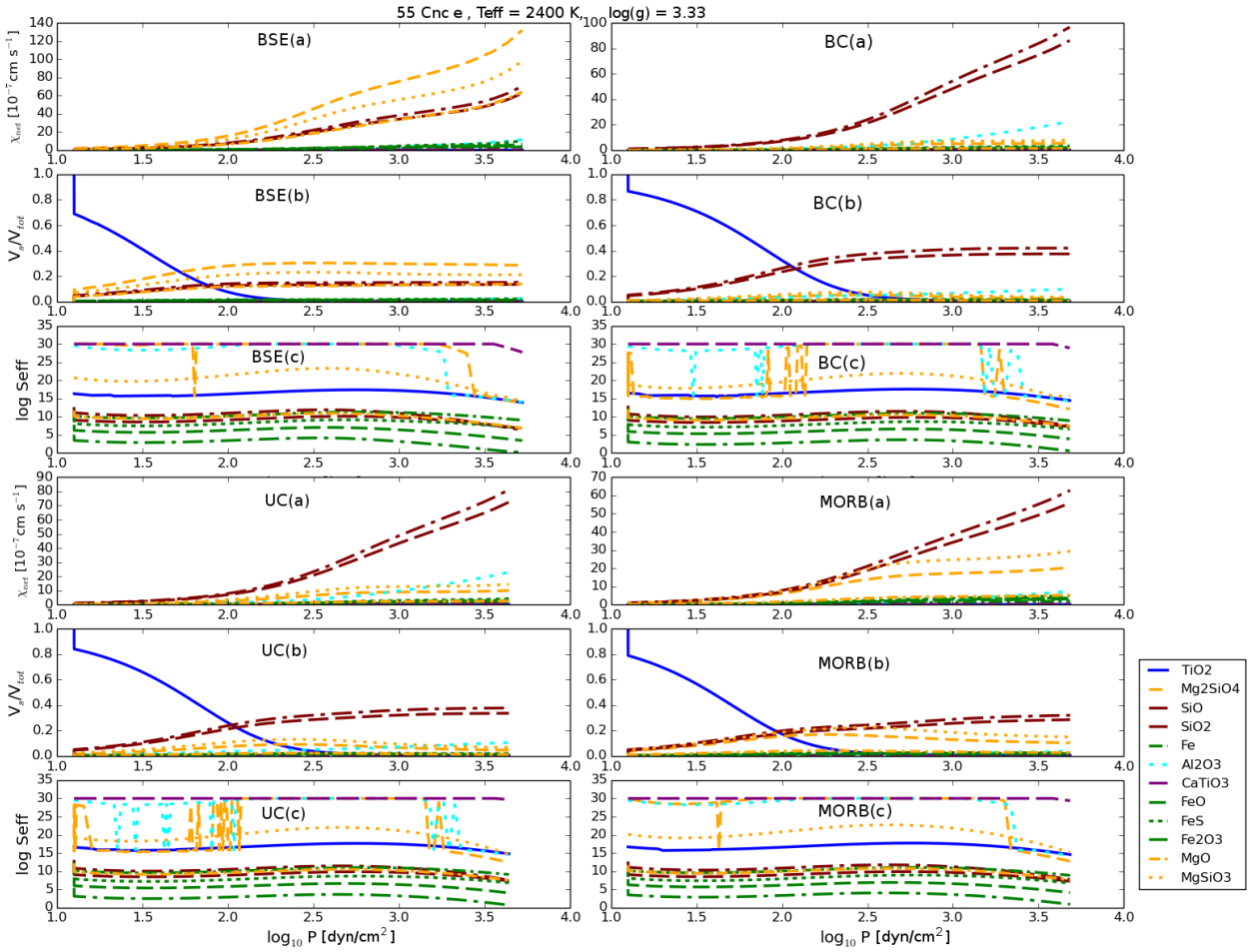

Figure 14: Showing the dust grain properties resulting from cloud formations on a sample atmosphere for 55 Cnc e (T_{eff}=2400K, logg=3.33) for four different compositions. **(a)** Individual grain growth velocity, χ_s [cm s^{-1}]; **(b)** Material volume fraction, V_s/V_{tot} [%]; **(c)** Effective supersaturation ratio, log Seff. The four compositions BSE, BC, UC, MORB have been labelled on each plot.

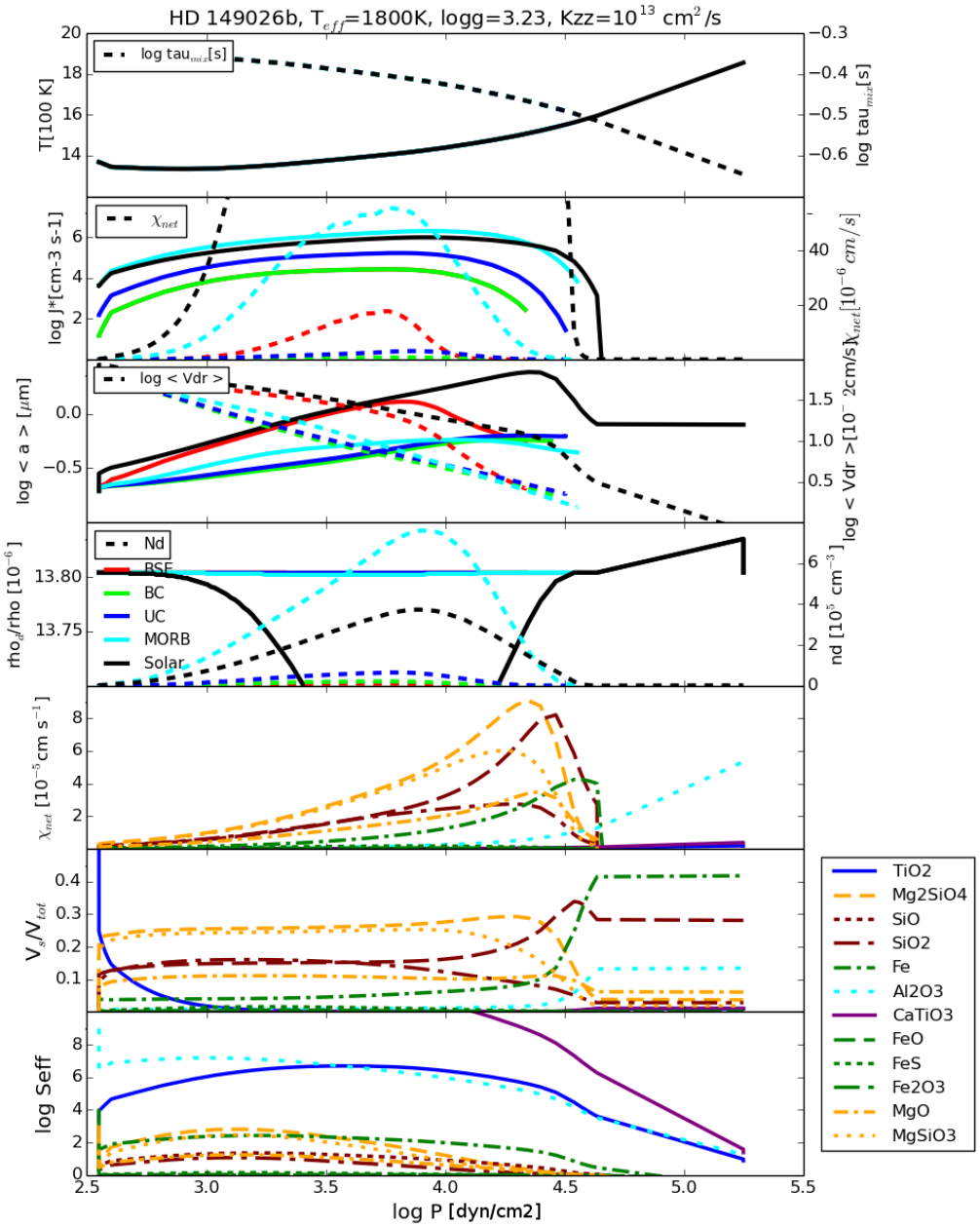

Figure 15: Showing the DRIFT cloud model results for HD149026b (T$_{eff}$=1800K,logg=3.23) atmosphere with varying compositions. **1st Panel:** local gas temperature, T$_{gas}$[K] (solid), Diffusive mixing time scale τ_{mix}[s] (dashed); **2nd Panel:** Nucleation rate, log J* (solid), dust growth rate χ_{net}; **3rd Panel:** Particle size, log $< a >$ [μm], Drift Velocity, log $< Vdr >$ [cm/s]; **4th Panel:** Dust density fraction, rho$_d$/rho, Particle number density, [cm^{-3}]. The cloud properties for five types of compositions are shown for each of the panels, Solar(Black), BSE(Red), Bulk Crust(Green), Upper Crust(Blue), MORB(Sky Blue). **5th Panel:** Individual grain growth velocity, χ_s [cm s^{-1}]; **6th Panel:** Material volume fraction, V$_s$/V$_{tot}$ [%]; **7th Panel:** Effective supersaturation ratio, log Seff.

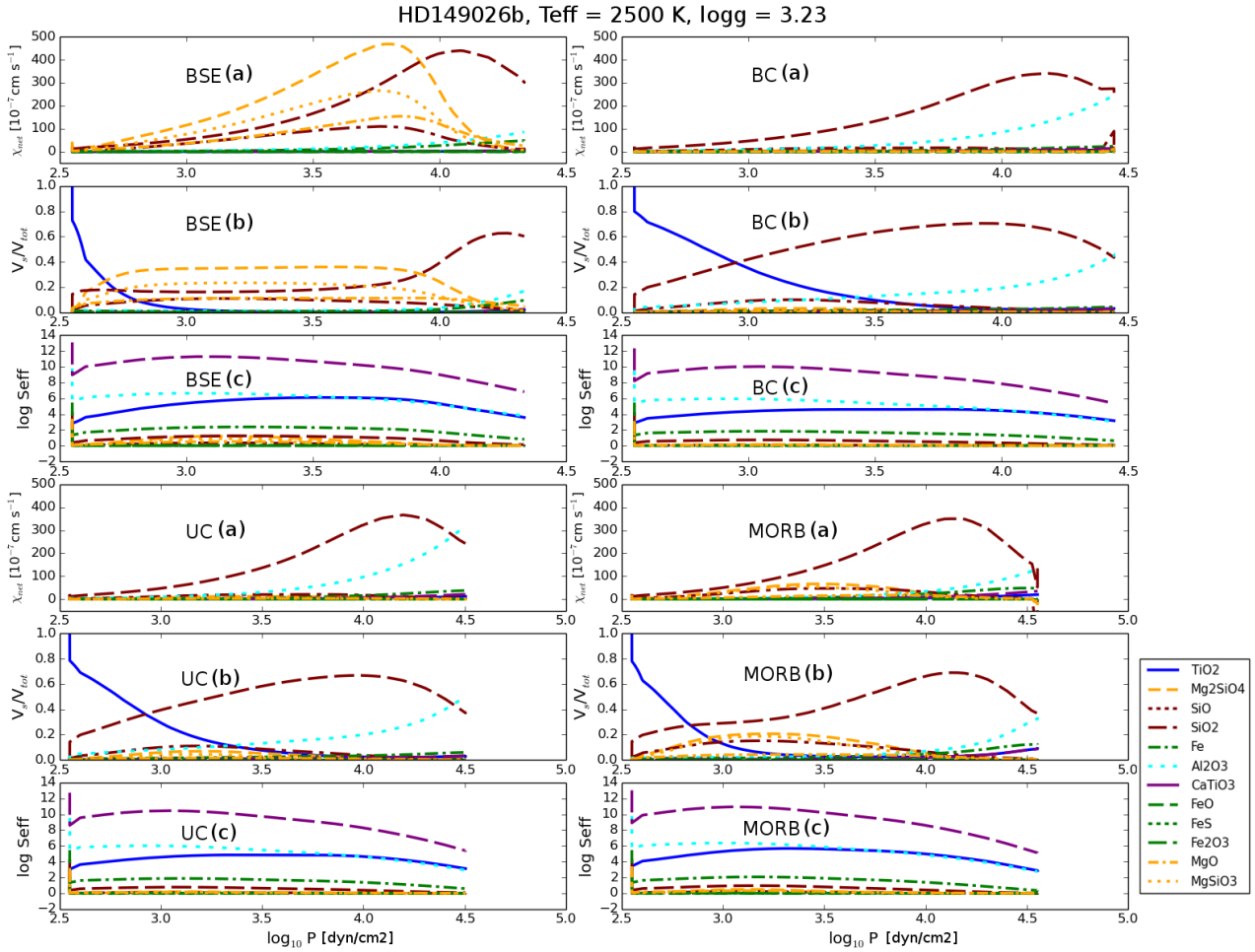

Figure 16: Showing the dust grain properties resulting from cloud formations on a sample atmosphere for HD149026b (T_{eff}=1800K, logg=3.23) for four different compositions. **(a)** Individual grain growth velocity, χ_s [cm s^{-1}]; **(b)** Material volume fraction, V_s/V_{tot} [%]; **(c)** Effective supersaturation ratio, log Seff. The four compositions BSE, BC, UC, MORB have been labelled on each plot.

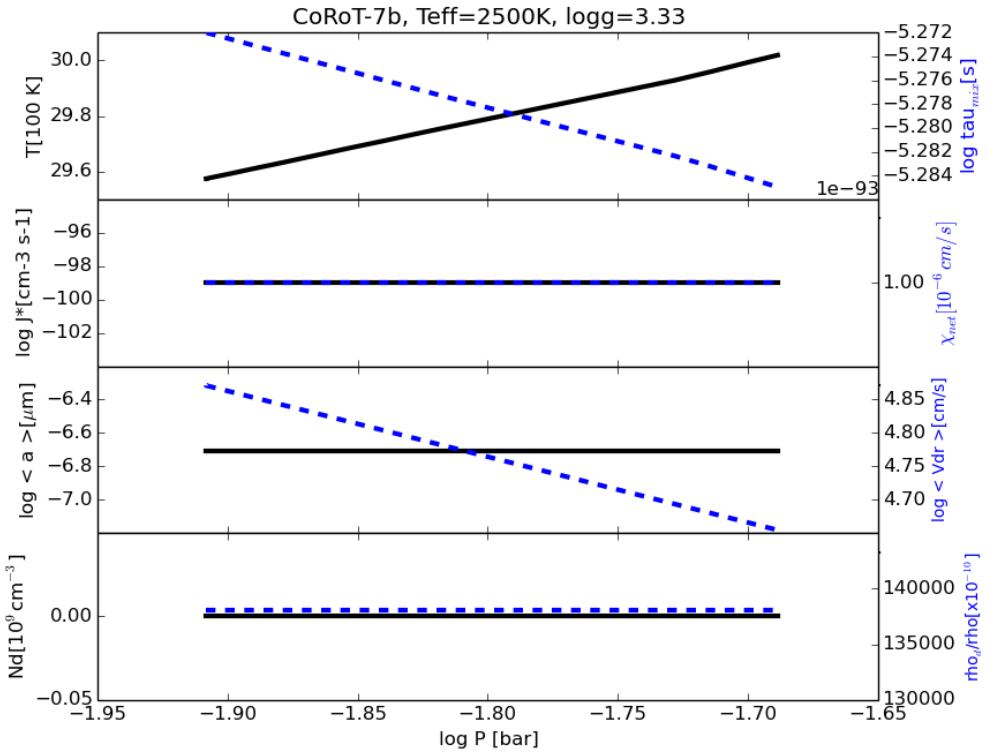

Figure 17: Showing the DRIFT cloud model results for CoRoT-7b (T_{eff}=2500K,logg=3.33).

References

M. Agúndez, V. Parmentier, O. Venot, F. Hersant, and F. Selsis. Pseudo 2d chemical model of hot-jupiter atmospheres: application to hd 209458b and hd 189733b. *Astronomy & Astrophysics*, 564:A73, 2014.

F. Allard and P. H. Hauschildt. Model atmospheres for m (sub) dwarfs: I. the base model grid. *arXiv preprint astro-ph/9601150*, 1996.

G. Bakos, R. Noyes, G. Kovács, D. Latham, D. Sasselov, G. Torres, D. Fischer, R. Stefanik, B. Sato, J. Johnson, et al. Hat-p-1b: A large-radius, low-density exoplanet transiting one member of a stellar binarybased in part on data collected at the subaru telescope, which is operated by the national astronomical observatory of japan. based in part on observations obtained at the wm keck observatory, which is operated by the university of california and the california institute of technology. keck time has been granted by nasa. *The Astrophysical Journal*, 656(1):552, 2007.

N. M. Batalha, W. J. Borucki, S. T. Bryson, L. A. Buchhave, D. A. Caldwell, J. Christensen-Dalsgaard, D. Ciardi, E. W. Dunham, F. Fressin, T. N. Gautier III, et al. Kepler's first rocky planet: Kepler-10bbased in part on observations obtained at the wm keck observatory, which is operated by the university of california and the california institute of technology. *The Astrophysical Journal*, 729(1):27, 2011.

C. Bilger, P. Rimmer, and C. Helling. Small hydrocarbon molecules in cloud-forming brown dwarf and giant gas planet atmospheres. *Monthly Notices of the Royal Astronomical Society*, page stt1378, 2013.

T. Castan and K. Menou. Atmospheres of hot super-earths. *The Astrophysical Journal Letters*, 743(2):L36, 2011.

B.-O. Demory, M. Gillon, D. Deming, D. Valencia, S. Seager, B. Benneke, C. Lovis, P. Cubillos, J. Harrington, K. Stevenson, et al. Detection of a transit of the super-earth 55 cancri e with warm spitzer. *Astronomy & Astrophysics*, 533:A114, 2011.

B.-O. Demory, M. Gillon, S. Seager, B. Benneke, D. Deming, and B. Jackson. Detection of thermal emission from a super-earth. *The Astrophysical Journal Letters*, 751(2):L28, 2012.

B.-O. Demory, M. Gillon, N. Madhusudhan, and D. Queloz. Variability in the super-earth 55 cnc e. *Monthly Notices of the Royal Astronomical Society*, 455(2):2018–2027, 2016.

A. L. Des Etangs, F. Pont, A. Vidal-Madjar, and D. Sing. Rayleigh scattering in the transit spectrum of hd 189733b. *Astronomy & Astrophysics*, 481(2):L83–L86, 2008.

B. Fegley Jr and K. Lodders. Atmospheric chemistry of the brown dwarf gliese 229b: Thermochemical equilibrium predictions. *The Astrophysical Journal Letters*, 472(1):L37, 1996.

J. Fortney, D. Saumon, M. Marley, K. Lodders, and R. Freedman. Atmosphere, interior, and evolution of the metal-rich transiting planet hd 149026b. *The Astrophysical Journal*, 642(1):495, 2006.

J. J. Fortney, M. S. Marley, and J. W. Barnes. Planetary radii across five orders of magnitude in mass and stellar insolation: application to transits. *The Astrophysical Journal*, 659(2):1661, 2007.

M. Gillon, B.-O. Demory, B. Benneke, D. Valencia, D. Deming, S. Seager, C. Lovis, M. Mayor, F. Pepe, D. Queloz, et al. Improved precision on the radius of the nearby super-earth 55 cnc e. *Astronomy & Astrophysics*, 539:A28, 2012.

N. Grevesse, M. Asplund, and A. Sauval. The solar chemical composition. *Space Science Reviews*, 130(1-4):105–114, 2007.

T. Guillot, A. Burrows, W. Hubbard, J. Lunine, and D. Saumon. Giant planets at small orbital distances. *The Astrophysical Journal Letters*, 459(1):L35, 1996.

C. Helling and S. Casewell. Atmospheres of brown dwarfs. *The Astronomy and Astrophysics Review*, 22(1):1–45, 2014.

C. Helling and P. Woitke. Dust in brown dwarfs. V. Growth and evaporation of dirty dust grains. *Aap*, 455:325–338, 2006a. ISSN 00046361. doi: 10.1051/0004-6361:20054598.

C. Helling and P. Woitke. Dust in brown dwarfs-v. growth and evaporation of dirty dust grains. *Astronomy & Astrophysics*, 455(1):325–338, 2006b.

C. Helling, P. Woitke, and W.-F. Thi. Dust in brown dwarfs and extra-solar planets-i. chemical composition and spectral appearance of quasi-static cloud layers. *Astronomy & Astrophysics*, 485 (2):547–560, 2008.

A. W. Howard, R. Sanchis-Ojeda, G. W. Marcy, J. A. Johnson, J. N. Winn, H. Isaacson, D. A. Fischer, B. J. Fulton, E. Sinukoff, and J. J. Fortney. A rocky composition for an earth-sized exoplanet. *Nature*, 503(7476):381–384, 2013.

Y. Ito, M. Ikoma, H. Kawahara, H. Nagahara, Y. Kawashima, and T. Nakamoto. Theoretical Emission Spectra of Atmospheres of Hot Rocky Super-Earths. *The Astrophysical Journal Letters*, 801:144, Mar. 2015. doi: 10.1088/0004-637X/801/2/144.

Y. Ito, M. Ikoma, H. Kawahara, H. Nagahara, Y. Kawashima, and T. Nakamoto. Theoretical emission spectra of atmospheres of hot rocky super-earths. *The Astrophysical Journal*, 801(2): 144, 2015.

H. A. Knutson, D. Charbonneau, L. E. Allen, J. J. Fortney, E. Agol, N. B. Cowan, A. P. Showman, C. S. Cooper, and S. T. Megeath. A map of the day–night contrast of the extrasolar planet hd 189733b. *Nature*, 447(7141):183–186, 2007.

H. A. Knutson, B. Benneke, D. Deming, and D. Homeier. A featureless transmission spectrum for the neptune-mass exoplanet gj [thinsp] 436b. *Nature*, 505(7481):66–68, 2014.

L. Kreidberg, J. L. Bean, J.-M. Désert, B. Benneke, D. Deming, K. B. Stevenson, S. Seager, Z. Berta-Thompson, A. Seifahrt, and D. Homeier. Clouds in the atmosphere of the super-earth exoplanet gj [thinsp] 1214b. *Nature*, 505(7481):69–72, 2014.

M. Kuzuhara, M. Tamura, T. Kudo, M. Janson, R. Kandori, T. Brandt, C. Thalmann, D. Spiegel, B. Biller, J. Carson, et al. Direct imaging of a cold jovian exoplanet in orbit around the sun-like star gj 504. *The Astrophysical Journal*, 774(1):11, 2013.

G. Lee, C. Helling, I. Dobbs-Dixon, and D. Juncher. Modelling the local and global cloud formation on hd 189733b. *Astronomy & Astrophysics*, 580:A12, 2015.

A. Léger, D. Rouan, J. Schneider, P. Barge, M. Fridlund, B. Samuel, M. Ollivier, E. Guenther, M. Deleuil, H. Deeg, et al. Transiting exoplanets from the corot space mission-viii. corot-7b: the first super-earth with measured radius. *Astronomy & Astrophysics*, 506(1):287–302, 2009.

N. Madhusudhan. C/o ratio as a dimension for characterizing exoplanetary atmospheres. *The Astrophysical Journal*, 758(1):36, 2012.

N. Madhusudhan, M. A. Amin, and G. M. Kennedy. Toward chemical constraints on hot jupiter migration. *The Astrophysical Journal Letters*, 794(1):L12, 2014.

N. Madhusudhan, M. Agúndez, J. I. Moses, and Y. Hu. Exoplanetary atmospheres—chemistry, formation conditions, and habitability. *Space Science Reviews*, pages 1–64, 2016.

W. McDonough and S. s. Sun. The composition of the earth. *Chemical Geology*, 120(3–4):223 – 253, 1995. ISSN 0009-2541. doi: http://dx.doi.org/10.1016/0009-2541(94)00140-4. Chemical Evolution of the Mantle.

Y. Miguel and L. Kaltenegger. Exploring atmospheres of hot mini-neptunes and extrasolar giant planets orbiting different stars with application to hd 97658b, wasp-12b, corot-2b, xo-1b, and hd 189733b. *The Astrophysical Journal*, 780(2):166, 2013.

Y. Miguel, L. Kaltenegger, B. Fegley, and L. Schaefer. Compositions of Hot Super-earth Atmospheres: Exploring Kepler Candidates. *The Astrophysical Journal Letters*, 742:L19, Dec. 2011. doi: 10.1088/2041-8205/742/2/L19.

Y. Miguel, L. Kaltenegger, B. Fegley, and L. Schaefer. Compositions of hot super-earth atmospheres: exploring kepler candidates. *The Astrophysical Journal Letters*, 742(2):L19, 2011a.

Y. Miguel, L. Kaltenegger, B. Fegley, and L. Schaefer. Compositions of hot super-earth atmospheres: exploring kepler candidates. *The Astrophysical Journal Letters*, 742(2):L19, 2011b.

J. I. Moses, C. Visscher, J. J. Fortney, A. P. Showman, N. K. Lewis, C. A. Griffith, S. J. Klippenstein, M. Shabram, A. J. Friedson, M. S. Marley, et al. Disequilibrium carbon, oxygen, and nitrogen chemistry in the atmospheres of hd 189733b and hd 209458b. *The Astrophysical Journal*, 737(1): 15, 2011.

B. E. Nelson, E. B. Ford, J. T. Wright, D. A. Fischer, K. von Braun, A. W. Howard, M. J. Payne, and S. Dindar. The 55 cancri planetary system: fully self-consistent n-body constraints and a dynamical analysis. *Monthly Notices of the Royal Astronomical Society*, 441(1):442–451, 2014.

H. Palme, K. Lodders, and A. Jones. Solar System Abundances of the Elements. *Treatise on Geochemistry: Second Edition*, 2:15–36, 2013. ISSN 0035922X. doi: 10.1016/B978-0-08-095975-7.00118-2.

V. Parmentier, A. P. Showman, and Y. Lian. 3d mixing in hot jupiters atmospheres-i. application to the day/night cold trap in hd 209458b. *Astronomy & Astrophysics*, 558:A91, 2013.

D. Perez-Becker and E. Chiang. Catastrophic evaporation of rocky planets. *Monthly Notices of the Royal Astronomical Society*, page stt895, 2013.

S. Rappaport, T. Barclay, J. DeVore, J. Rowe, R. Sanchis-Ojeda, and M. Still. Koi-2700b—a planet candidate with dusty effluents on a 22 hr orbit. *The Astrophysical Journal*, 784(1):40, 2014.

B. Sato, D. A. Fischer, G. W. Henry, G. Laughlin, R. P. Butler, G. W. Marcy, S. S. Vogt, P. Bodenheimer, S. Ida, E. Toyota, et al. The n2k consortium. ii. a transiting hot saturn around hd 149026 with a large dense corebased on data collected at the subaru telescope, which is operated by the national astronomical observatory of japan. based on observations obtained at the wm keck observatory, which is operated by the university of california and the california institute of technology. keck time has been granted by noao and nasa. *The Astrophysical Journal*, 633(1): 465, 2005.

L. Schaefer and B. Fegley. A thermodynamic model of high temperature lava vaporization on Io. *icarus*, 169:216–241, May 2004. doi: 10.1016/j.icarus.2003.08.023.

L. Schaefer and B. Fegley. A thermodynamic model of high temperature lava vaporization on io. *Icarus*, 169(1):216–241, 2004.

L. Schaefer and B. Fegley. Chemistry of silicate atmospheres of evaporating super-earths. *The Astrophysical Journal Letters*, 703(2):L113, 2009a.

L. Schaefer and B. Fegley. Chemistry of silicate atmospheres of evaporating super-earths. *The Astrophysical Journal Letters*, 703(2):L113, 2009b.

I. A. Snellen, E. J. de Mooij, and S. Albrecht. The changing phases of extrasolar planet corot-1b. *Nature*, 459(7246):543–545, 2009.

S. R. Taylor and S. McLennan. *Planetary Crusts: Their Composition, Origin and Evolution*. Jan. 2009.

O. B. Toon, C. McKay, T. Ackerman, and K. Santhanam. Rapid calculation of radiative heating rates and photodissociation rates in inhomogeneous multiple scattering atmospheres. *Journal of Geophysical Research: Atmospheres*, 94(D13):16287–16301, 1989.

A. Tsiaras, M. Rocchetto, I. Waldmann, O. Venot, R. Varley, G. Morello, G. Tinetti, E. Barton, S. Yurchenko, and J. Tennyson. Detection of an atmosphere around the super-earth 55 cancri e. *arXiv preprint arXiv:1511.08901*, 2015.

T. Tsuji. Molecular abundances in stellar atmospheres. ii. *Astronomy and Astrophysics*, 23:411–431, 1973.

D. Valencia, D. D. Sasselov, and R. J. O'Connell. Detailed models of super-earths: how well can we infer bulk properties? *The Astrophysical Journal*, 665(2):1413, 2007.

O. Venot, E. Hébrard, M. Agùndez, M. Dobrijevic, F. Selsis, F. Hersant, N. Iro, and R. Bounaceur. A chemical model for the atmosphere of hot jupiters. *Astronomy & Astrophysics*, 546:A43, 2012.

J. N. Winn, J. M. Matthews, R. I. Dawson, D. Fabrycky, M. J. Holman, T. Kallinger, R. Kuschnig, D. Sasselov, D. Dragomir, D. B. Guenther, et al. A super-earth transiting a naked-eye starbased on data from the most satellite, a canadian space agency mission, jointly operated by dynacon inc., the university of toronto institute for aerospace studies, and the university of british columbia, with the assistance of the university of vienna. *The Astrophysical Journal Letters*, 737(1):L18, 2011.

P. Woitke and C. Helling. Dust in brown dwarfs-ii. the coupled problem of dust formation and sedimentation. *Astronomy & Astrophysics*, 399(1):297–313, 2003.

P. Woitke and C. Helling. Dust in brown dwarfs-iii. formation and structure of quasi-static cloud layers. *Astronomy & Astrophysics*, 414(1):335–350, 2004.